Master's thesis

NTNU
Norwegian University of Science and Technology
Faculty of Engineering
Department of Energy and Process Engineering

Henrik Plassen

# Integration of R744 and R290 Heat Pumps for Two-family Houses

Master's thesis in Mechanical Engineering
Supervisor: Armin Hafner
Co-supervisor: Christian Schlemminger
June 2022

NTNU
Norwegian University of
Science and Technology

Henrik Plassen

# Integration of R744 and R290 Heat Pumps for Two-family Houses

Master's thesis in Mechanical Engineering
Supervisor: Armin Hafner
Co-supervisor: Christian Schlemminger
June 2022

Norwegian University of Science and Technology
Faculty of Engineering
Department of Energy and Process Engineering

NTNU
Norwegian University of
Science and Technology

# Preface

The work in this master's thesis was carried out in the spring of 2022 and is a continued work on the project thesis of fall 2021. The work comprises of 30 ECTS credits and is conducted at the Department of Energy and Process Engineering, Norwegian University of Science and Technology. My study is Mechanical Engineering, and main profile is Industrial Process Technology.

The last couple of years has been quite memorable, with a national community lockdown resulting in home office, away office and new ways of socialising. Also, during the master's work, the community has reopened, and study halls are again filled with students. I am grateful I have been able to perform the work largely as planned, and the lockdown has had little direct effect on the work.

First, I would like to thank my supervisor Professor Armin Hafner for believing in me and always staying positive and optimistic, giving specific feedback with high professionality. I would also like to thank Winns and Per Alsvik for their help in work with automating and increasing heat pump controls for further testing. Lastly, a special thanks to Anna and Frost for being fantastic and disrupting me in my thesis work.

# Abstract

Domestic hot water (DHW) and space heating are significant energy demands consuming most of the energy delivered to residential buildings in colder climates. Heat pumping systems utilise surrounding energy to reduce the use of electrical power. Today the utilisation of heat pumps for DHW and space heating is limited, largely due to limitations in conventional heat pumps and accessibility. Standardising contemporary heat pumps with natural refrigerants, capable of also heating DHW for use in residential buildings, can, therefore, significantly reduce the electrical power consumption in colder climates and, in turn, reduce $CO_2$ emissions.

This report describes the methods of creating a digital heat pump system replica in Dymola to simulate and analyse the effects of changes to boundary conditions or the implementation of new hardware and software. The heat pumping system covers DHW and space heating demands with natural working fluids, a carbon dioxide (R744/$CO_2$) heat pump heating both hydronic and domestic hot water and a propane (R290) heat pump reheating hydronic supply water. Documenting the performance of these systems can be used to further develop standardised heat pumps for space and DHW heating in residential buildings.

# Norwegian summary

Forbruk av varmt tappevann og romoppvarming er store energiposter, og står for det meste av energien som leveres til boliger i kalde klima. Varmepumpesystemer utnytter energi i omgivelsene for å redusere bruk av elektrisk strøm til oppvarming. I dag er bruken av varmepumper for oppvarming av varmt tappevann utilstrekkelig, mye grunnet begrensninger i de konvensjonelle varmepumpene på markedet. Å standardisere fremtidsrettede varmepumper med naturlige kjølemedier, for boliger, kapable til å dekke behovet for varmt tappevann og romoppvarming kan derfor sterkt redusere behovet for elektrisk energi i kaldere klima, og med det redusere $CO_2$ utslipp.

Denne rapporten beskriver metodene for å lage en digital replika av et varmepumpesystem i Dymola for å kunne simulere og analysere effekter av endringer i grensebetingelser eller implementering av ny maskinvare og programvare. Varmepumpesystemet dekker behov til rom- og tappevannsoppvarmingmed naturlige kjølemedier, en karbondioksid (R744/$CO_2$) varmepumpe som varmer tappevann og gulvvarme, og en propan (R290) varmepumpe som løfter temperaturen på tur-vannet ved behov. Kartlegging av ytelsen til disse oppvarmingssystemene kan bruker til å videre utvilke standardiserte varmepumper for rom- og varmtvannsoppvarming i boligbygg.

# Table of Contents

# List of Figures

# List of Tables

# Nomenclature

## Latin symbols

| | | |
|---|---|---|
| $A$ | Area | $\mathrm{m}^2$ |
| $c_p$ | Isobaric specific heat capacity | $\mathrm{J\,kg^{-1}\,K^{-1}}$ |
| $h$ | Convection heat transfer coefficient | $\mathrm{W\,m^{-2}\,K^{-1}}$ |
| $\dot{m}$ | Mass flow | kg |
| $p$ | Pressure | Pa |
| $\dot{q}$ | Heat flux | $\mathrm{W\,m^{-2}}$ |
| $\dot{Q}$ | Heat flow | W |
| $U$ | Overall heat transfer coefficient | $\mathrm{W\,m^{-2}\,K}$ |
| $R$ | Thermal heat resistance | $\mathrm{K\,W^{-1}\,m^{-2}}$ |
| $v$ | Specific volume | $\mathrm{m^3\,kg^{-1}}$ |

## Greek symbols

| | | |
|---|---|---|
| $\kappa$ | Isentropic Exponent | |
| $\rho$ | Density | $\mathrm{kg\,m^{-3}}$ |
| $\pi$ | Pressure ratio | |

## Abbreviations

| | |
|---|---|
| DHW | Domestic hot water |
| COP | Coefficient of performance |
| CFC | Chlorofluorocarbons |
| HFC | Hydrofluorocarbons |
| HP | Heat pump |
| $CO_2$ | Carbon dioxide |
| SPF | Seasonal Performance Factor |
| SGHX | Suction gas heat exchanger |
| GC | Gas cooler |
| LPR | Low pressure receiver |

### Subscripts

| | |
|---|---|
| $i$ | Inlet |
| $e$ | Outlet |
| $E$ | Evaporator |
| $C$ | Condenser |
| $is$ | Isentropic |
| $ad$ | Adiabatic |
| $gc$ | Gas cooler |
| $h$ | Heating |
| $R$ | Refrigerant |

# 1 Introduction

The Kyoto Protocol states that hydrofluorocarbons (HFC) need to be replaced due to the negative impact on the greenhouse effect.[1] Safe alternatives are natural working fluids, such as carbon dioxide ($CO_2$/R744), propane (R290) and ammonia (R717). The working fluids considered in this report are propane and $CO_2$.

The annual energy use in Norwegian residential buildings was in 2020 46 TW h and 21.6 % of the total energy consumption.[2] Of this, 78 % is used for domestic hot water and space heating, making the impact on total energy use from optimising the heating and cooling of buildings significant.[3] A part of this optimisation could be an increase in the use of R744 and R290 in heat pumps.

R744 as a refrigerant is practically perfect. It does not contribute to global warming or ozone depletion; it is non-toxic, non-flammable, inexpensive and compatible with standard machine materials.[4] The refrigerant is well suited for DHW heating and a combination of DHW and space heating. Results show that R744 can outperform R410A in combined heating when the ratio between space and water heating is low ($< 0.6$ to 1.0).[5] R290 is a refrigerant capable of delivering heat at relatively high temperatures with acceptable efficiency and is shown to be a favourable replacement for R134a.[6]

**The Master's Agreement** states tasks to be considered in the continued work. This includes a literature review of R290 and R744 heat pump systems, further development of the Dymola models, an evaluation of system performance through Dymola simulations and/or measurements, and a summary report presenting findings and discussion. Throughout this thesis, much work has been made to facilitate further testing and modifications to the heat pump system.

**The R744 Heat Pump** installed at the two-family house is a product of near 20 year old technology. Heat pumps are under constant development and highly current with the ambitions for lower power consumption and gas dependency. One of these improvements is the introduction of multi-ejectors, reducing the relatively large throttling losses in R744 systems.[7]

# 2 Theory

This section aims to give the reader insight into the heat pumping technology and the working fluids used. The tri-partite gas cooler will be further explained, and the reader will be given knowledge about the heat sources and heat sinks of the system at hand.

## 2.1 Heat Pumping System

A heat pump transports heat from a low-temperature source to a high-temperature sink using compression work (fig. 2.1).

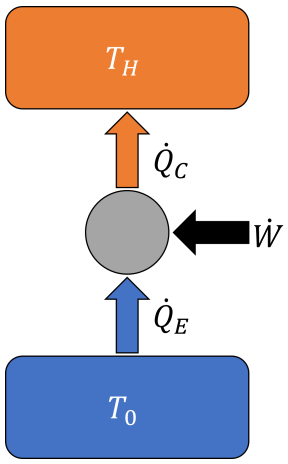


Figure 2.1: Principle sketch showing a heat pump extracting heat from a low-temperature heat source and delivering heat to a high-temperature heat sink by use of work.

This is done by compressing a working fluid for high-temperature heat release and then expanding the fluid for low-temperature heat capture (fig. 2.2). The process can be explained in four steps:

- 1 $\longrightarrow$ 2: The gas is compressed through the compressor, increasing the temperature and pressure of the fluid.
- 2 $\longrightarrow$ 3: The superheated gas is first cooled down to the saturated gas line before condensing to the saturated liquid line. This process releases a large amount of heat per mass working fluid at near constant temperature, as indicated by the change in specific enthalpy (fig. 2.2b).
- 3 $\longrightarrow$ 4: The liquid is now expanded, lowering the pressure and temperature, creating a two-phase state of gas and liquid. This process induces negligible changes in enthalpy.
- 4 $\longrightarrow$ 1: Heat is extracted from the heat source as the working fluid evaporates in the evaporator to or past the saturated gas line.

Drawing a control volume around the evaporator and performing an energy balance results in a relation between refrigerant enthalpy, mass flow and heat extracted from heat source (1).

$$\dot{Q}_E = \dot{m}_R(h_1 - h_4) \tag{1}$$

Doing the same procedure on the condenser results in an equivalent relation (2).

$$\dot{Q}_C = \dot{m}_R(h_2 - h_3) \tag{2}$$

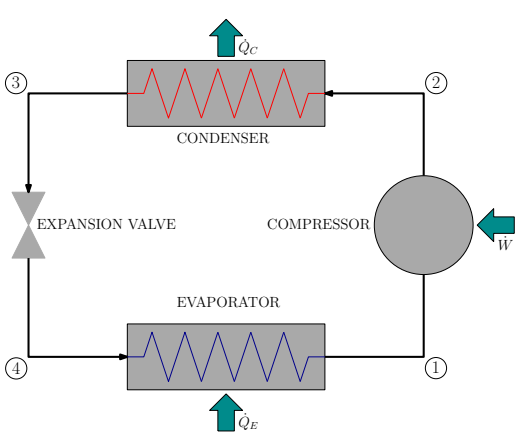


(a) A heat pumping system with principal components and energy flow.

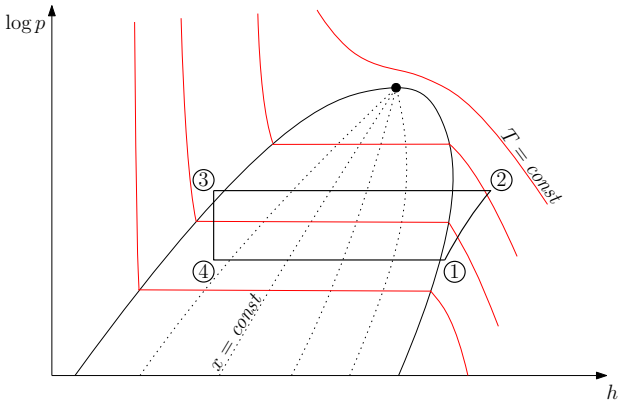


(b) Pressure - enthalpy diagram with a principle heat pumping cycle. The dotted grey line shows a constant liquid/gas fraction, ($x$).

Figure 2.2: A principle heat pumping cycle with state points 1 to 4.

The compression from state point 1 to state point 2 would ideally be isentropic, giving state point $2_{is}$ (fig. 2.3). Due to efficiency losses, the compressor will use more energy than needed, increasing the enthalpy and temperature. With no heat loss, the compression would be adiabatic, and all energy would enter the gas, giving state point $2_{ad}$.

The difference in work required to compress the gas from the evaporating pressure, $p_E$, to the condensing pressure, $p_C$, is expressed with the isentropic efficiency factor, $\eta_{is} \in [0, 1]$ (3).

$$\dot{w} = \frac{\dot{w}_{is}}{\eta_{is}} \tag{3}$$

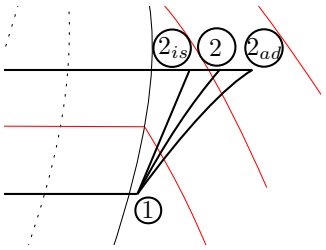


Figure 2.3: Principle sketch of compression lines as part of figure 2.2b. Compression lines from left to right: isentropic compression, real compression and adiabatic compression.

## 2.2 Working Fluids

To better understand the heat pumping process, it is helpful to be familiar with the $\log p - h$ diagram (fig 2.4). This part will also introduce the two working fluids, propane and carbon dioxide. As refrigerants, these are named R290 and R744, respectively. These are natural workings fluids with low global warming potential (GWP) and zero ozone depletion potential (ODP).

The $\log p - h$ diagram is commonly used to evaluate refrigerant cycles. The different phases are clearly stated, and comparing the horizontal lengths of each line gives a good indication of how well the system is performing.

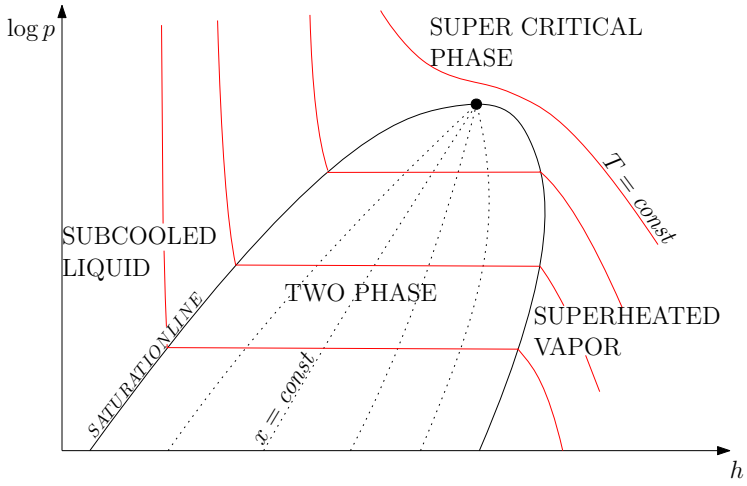


Figure 2.4: Phase diagram for working fluids. Dotted lines show constant liquid/gas fraction, $x$. Constant temperature lines are red, and the critical point is marked as a black dot.

The coefficient of performance ($COP$) is defined as the ratio between useful heat and work provided (4). In a heat pumping process, the useful heat is rejected heat, while in a refrigerating system, absorbed heat is useful. In a combined system, both absorbed and rejected heat is useful.

$$COP_h = \frac{\dot{Q}_C}{\dot{W}} = \frac{h_2 - h_3}{h_{2_{ad}} - h_1} \tag{4}$$

### 2.2.1 R290 - Propane

Propane has quite similar thermodynamic properties to R134a and operates at moderate pressure levels. In ambient temperature and pressure, the fluid is in gaseous form, highly flammable and explosive, but nontoxic. The gas is colour- and odourless, unlike propane used for combustion, which is given an odour additive. Table 2.1 provides important fluid properties.

Table 2.1: Fluid properties of R290 (saturation temperature 0 °C).

| Properties | R290 | |
|---|---|---|
| Molecular weight | 44.1 | $\mathrm{kg\,kmol^{-1}}$ |
| Critical temperature | 96.6 | °C |
| Critical pressure | 42.3 | bar |
| Thermal conductivity, liquid | 104.7 | $10^{-3}\,\mathrm{W\,m^{-1}\,K^{-1}}$ |
| Thermal conductivity, gas | 15.4 | $10^{-3}\,\mathrm{W\,m^{-1}\,K^{-1}}$ |
| Kinematic viscosity, liquid | 233.5 | $10^{-3}\,\mathrm{m^2\,s^{-1}}$ |
| Kinematic viscosity, gas | 748.2 | $10^{-3}\,\mathrm{m^2\,s^{-1}}$ |
| Volumetric capacity | 3862.8 | $\mathrm{kJ\,m^{-3}}$ |
| GWP | 3 | |
| ODP | 0 | |
| Flammability | Highly flammable | |

### 2.2.2 R744 - Carbon Dioxide

Carbon dioxide (R744) is one of the first refrigerants used in mechanical refrigeration systems before Chlorofluorocarbons (CFC) and hydrofluorocarbons (HFC) took over. Later, R744 has been revived as a refrigerant, being near an ideal refrigerant [4]. R744 is shown able to outperform R410A when the ratio between space and water heating is lower than 0.6-1.0 and the heat source is colder than 20 °C [5].

Table 2.2: Fluid properties of R744 (saturation temperature 0 °C).

| Properties | R744 | |
|---|---|---|
| Molecular weight | 44.0 | $\mathrm{kg\,kmol^{-1}}$ |
| Critical temperature | 31.1 | °C |
| Critical pressure | 73.8 | bar |
| Thermal conductivity, liquid | 111.0 | $10^{-3}\,\mathrm{W\,m^{-1}\,K^{-1}}$ |
| Thermal conductivity, gas | 18.7 | $10^{-3}\,\mathrm{W\,m^{-1}\,K^{-1}}$ |
| Kinematic viscosity, liquid | 108.0 | $10^{-3}\,\mathrm{m^2\,s^{-1}}$ |
| Kinematic viscosity, gas | 150.9 | $10^{-3}\,\mathrm{m^2\,s^{-1}}$ |
| Volumetric capacity | 22 519.5 | $\mathrm{kJ\,m^{-3}}$ |
| GWP | 1 | |
| ODP | 0 | |
| Flammability | Nonflammable | |

With a critical temperature of 31.1 °C, R744 will in most heat pump applications need to reject heat in the supercritical phase (fig 2.4). This means the gas will be cooled and not condensed, having a gliding temperature. The gas should be cooled sufficiently to achieve the highest possible COP, giving less flash gas and a larger portion of heat added through the evaporator. An experimental result shows a $\mathrm{COP}_h$ increase of about 12.5 % when decreasing water inlet temperature from 25 °C to 15 °C, with a water outlet temperature of 65 °C and without internal heat exchanger [8]. R744 is therefore well fitted for heating domestic hot water [9]. Table 2.2 provides important fluid properties.

## 2.3 Tri-partite gas cooler

The tri-partite gas cooler is a heat exchanger (HE) configuration where three heat exchangers are connected in series, dividing the heat rejection into sections of high, medium and low temperature. The high-temperature HE, now called GC1, reheats the domestic hot water (DHW) to the desired temperature. The low-temperature HE, GC3, preheats the DHW and the medium temperature HE, GC2, heats the space heating system. Experimental results from a tri-partite plate heat exchanger configuration show that the thermal resistance on the $CO_2$ side is the main factor influencing the heat transfer [10].

## 2.4 Heat Sources

The purpose of the heat source is to supply heat to the evaporator. As the compressor work is strongly affected by the pressure ratio, $\pi$, a higher brine temperature will give a higher $COP$. This paper will introduce the ambient air, ventilation exhaust and the ground heat sources, as the ground source is in use and ambient air and ventilation exhaust heat sources are being installed. Other heat sources are seawater, freshwater, wastewater and waste heat (industry).

### 2.4.1 Ambient Air Heat Source

Ambient air has large fluctuations in temperature, both daily and yearly. On the other hand, the investment costs of an ambient heat source are relatively small. As a space heating heat source, the heat demand and heat source temperature are inversely proportional. Still, as domestic hot water consumption is more constant throughout the year, ambient air is preferable in warmer months in buildings with no cooling demand.

### 2.4.2 Ground Heat Source

The temperature in a ground heat source is highly stable, giving good operating conditions for the heat pump throughout the year. The temperature stability gives a relatively low source temperature in the summer and a high source temperature in the winter when space heating demand is high. The relatively low temperature during summer also facilitates the use of borehole heat exchangers as heat sinks when there is need for cooling. This can, in some cases, charge the ground with energy, giving better working conditions in the heating season. Because of the temperature variations in the ground and ambient air, a combination of both, using air in the summer and ground heat in the winter, gives a higher overall source temperature. This also decreases the load on the ground heat source while facilitating the possibility of charging the ground with ambient air heat.

### 2.4.3 Ventilation Exhaust Air

The ventilation exhaust air has a quite high temperature and carries a large amount of energy. Usually, the heat is recovered through a rotary heat exchanger with a high efficiency, leaving little energy for the heat pump to extract. The exhaust air heat source is most applicable in renovations where exhaust ventilation is already installed, and upgrading to balanced ventilation with heat recovery is impractical or expensive.

## 2.5 Heat Distributors/Sinks

Heat sinks in residential buildings are essentially space heating and hot water heating systems. The hot water system has a large temperature difference, with an inlet temperature of about 10 °C and outlet temperature above 55 °C. Floor heating systems, on the other hand, usually have a supply/return temperature difference around 5 °C.

### 2.5.1 Domestic Hot Water Heating System

As the DHW use is somewhat lower in the summer and the cold water temperature is lower in the winter, the DHW load is highest in the winter. A DHW load of $16.1\,\mathrm{kW\,h\,m^{-2}\,yr^{-1}}$ is measured in a multi-family building.[11] The hot tap water is stored in accumulator tanks to cope with and smoothen high peak demands. To keep a low cold water (CW) temperature entering the heat pump, two effects should reduced. Water mixing in the storage tanks is reduced, this can be done with a diffuser at inlets and outlets. Conduction and convection can be lowered through use of multiple storage tanks in series, to maintain a lower temperature gradient, $dT/dy$. Storage tanks in series is shown connected in chapter 3.

### 2.5.2 Hydronic Space Heating / Hydronic Heating Systems

Hydronic space heating systems circulate water between their heat source and heat rejectors such as radiators, convectors and floor heating. To facilitate high heat pump efficiency, the circulating water temperature should be low and with a low supply/return temperature difference. This demands a low heat resistance between the hydronic water and the room, meaning surface area and/or convection heat transfer must be increased. Energy use for space heating is proportional to the outdoor temperature to the point of no heat demand. The heat load for space heating varies greatly with the year of construction as insulation requirements have been modified over time.

# 3 System Description

This section aims to describe the two systems at hand and provide the reader with the system information needed to understand the following sections.

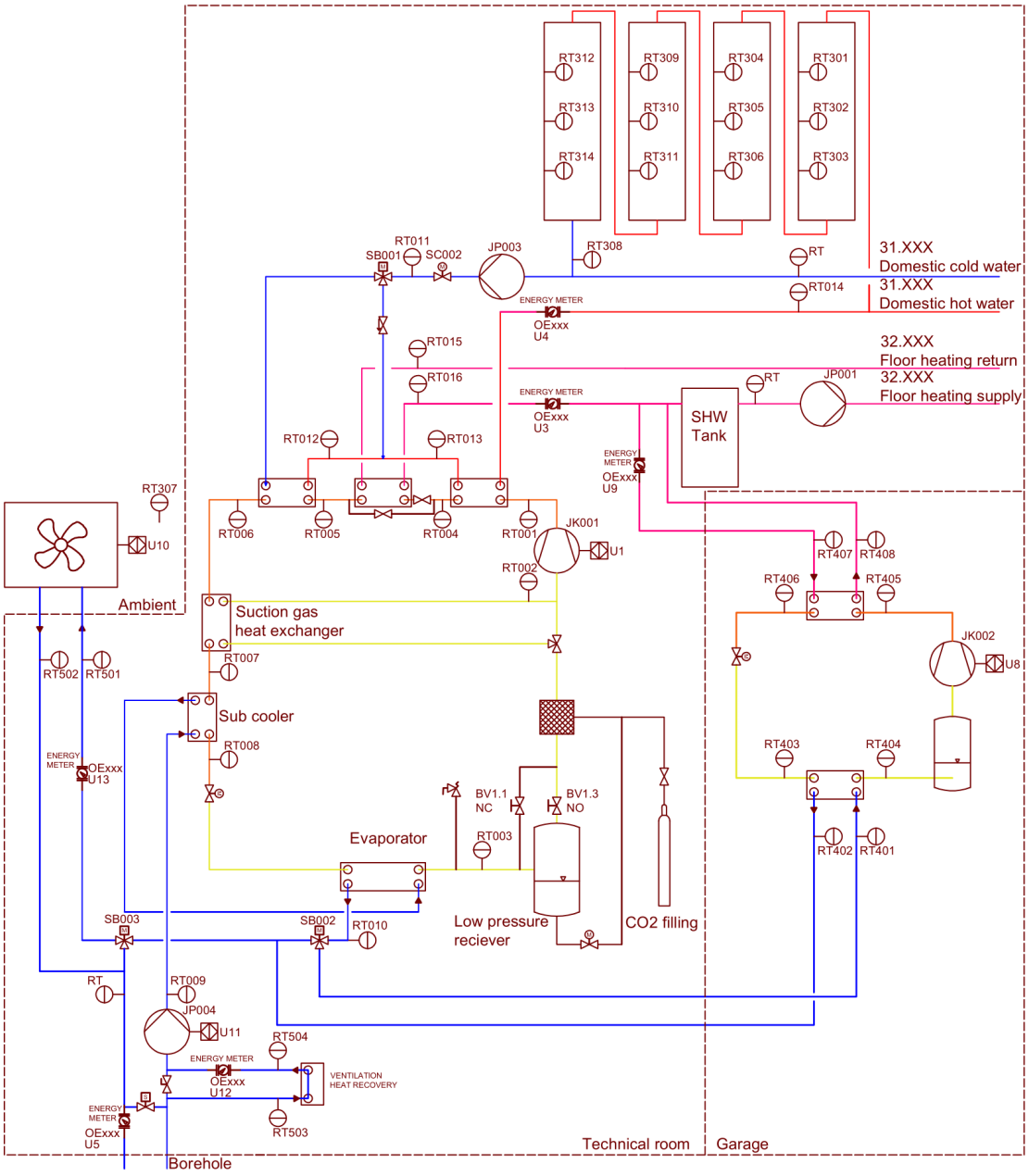


Figure 3.1: Piping and instrumentation diagram (P&ID) showing the heat pumps connected to the heat sources and heat sinks. Blue lines are brine and cold water; red lines are hot water; orange lines are high-pressure fluid pipes, and yellow lines are low-pressure fluid pipes.

## 3.1 R744 Heat Pump Structure

In addition to the standard heat pump components shown in the preceding section, the R744 heat pump (HP) at hand has a suction gas heat exchanger, sub cooler and a low-pressure receiver (fig. 3.1). Heat rejection in the R744 HP happens through the tube-in-tube tri-partite gas cooler, consisting of a DHW reheater, preheater and a space heating gas cooler.

### 3.1.1 Evaporator

The evaporator is a counterflow tube-in-tube heat exchanger with R744 in the inner tube ($D_i = 8\,\text{mm}$) and brine through the outer tube ($D_i = 20\,\text{mm}$). The stainless steel tubes are 12 m with an average coil diameter of 450 mm.

Table 3.1: Evaporator technical specifications. [12]

| Type | Tube-in-tube heat exchanger |
|---|---|
| Material | Stainless steel |
| Diameters, $CO_2$ tube | $D_i = 8\,\text{mm}$ |
| | $D_o = 10\,\text{mm}$ |
| Diameters, brine tube | $D_i = 20\,\text{mm}$ |
| | $D_o = 24\,\text{mm}$ |
| Tube length | 12 m |
| Average coil diameter | 450 mm |
| Approximate weight | 17 kg |
| Heat transfer area, $CO_2$ side | $A_i = 0.302\,\text{m}^2$ |
| Heat transfer area, brine side | $A_o = 0.377\,\text{m}^2$ |
| Heat transfer area ratio | $A_o/A_i = 1.25$ |
| Cross sectional area, inner tube | $A_{c,i} = 50\,\text{mm}^2$ |
| Cross sectional area, annuli tube | $A_{c,o} = 236\,\text{mm}^2$ |

### 3.1.2 Compressor

The compressor is a Dorin R744 compressor, model CD180H, a semi-hermetic reciprocating compressor. Given compressor data is presented in table 3.2.

Table 3.2: R744 compressor data.

| Parameter | |
|---|---|
| Model | CD180H |
| $PS$ | 150 bar |
| $PS_S$ | 100 bar |
| Voltage | 230 V |
| Phase | 3 |
| Frequency | 50 |
| RPM | 1450 |

### 3.1.3 Gas Coolers

The gas coolers are connected in series, creating a tri-partite gas cooler. The $CO_2$ fluid first enters the DHW reheating gas cooler (GC1) and, lastly, exits the preheating gas cooler (GC3). All three gas coolers are stainless steel tube-in-tube and coiled with an average coil diameter from 350 mm to 450 mm. The reheating gas coolers function is to heat tap water above 60 °C. GC1 is, with its 3.5 m length, the shortest of the three gas coolers. The space heating gas cooler (GC2) is the largest of the three gas coolers, with a tube length of 15 m and weighing approximately 18 kg. GC3 is approximately four times as large as the reheating GC and lowers the $CO_2$ fluid temperature to a minimum. For further details see table 3.3.

Table 3.3: Tripartite gas cooler technical specifications. [12]

| Parameter | Tube-in-tube heat exchanger | | |
|---|---|---|---|
| | GC1 | GC2 | GC3 |
| Material | Stainless steel | Stainless steel | Stainless steel |
| Diameters, $CO_2$ tube | | | |
| Inner diameter, $D_i$ | 6 mm | 6 mm | 6 mm |
| Outer diameter, $D_o$ | 8 mm | 8 mm | 8 mm |
| Diameters, brine tube | | | |
| Inner diameter, $D_i$ | 12 mm | 12 mm | 12 mm |
| Outer diameter, $D_o$ | 16 mm | 16 mm | 16 mm |
| Tube length | 3.5 m | 15 m | 14 m |
| Average coil diameter | 350 mm | 450 mm | 350 mm |
| Approximate weight | 3 kg | 18 kg | 13 kg |
| Heat transfer area | | | |
| $CO_2$ side, $A_i$ | 0.067 $m^2$ | 0.283 $m^2$ | 0.264 $m^2$ |
| Brine side, $A_o$ | 0.088 $m^2$ | 0.377 $m^2$ | 0.352 $m^2$ |
| Heat transfer area ratio, $A_o/A_i$ | 1.33 | 1.33 | 1.33 |
| Cross sectional area | | | |
| Inner tube, $A_{c,i}$ | 28 $mm^2$ | 28 $mm^2$ | 28 $mm^2$ |
| Annuli tube, $A_{c,o}$ | 63 $mm^2$ | 204 $mm^2$ | 63 $mm^2$ |

## 3.2 R290 Heat Pump Structure

The R290 is a standardised heat pump with two plate heat exchangers and a piston compressor. The compressor is delivered by GEA Bock GmbH, and details are listed in table 3.4. No further product details are given by the distributor.

Table 3.4: R290 compressor data.

| Model | HG12P / 75-4 S HC |
|---|---|
| Nr | BC48617A046 |
| $I_{max}$ | 8.0/4.6A |
| $I_{block}$ Δ | 43 A |
| $I_{block}$ ⅄ | 25 A |
| $p_{max}$ | 19/28bar |
| $f$ | 50 Hz |
| $n$ | 1450 $min^{-1}$ |
| $\dot{V}_{th}$ | 6.7 $m^3\,h^{-1}$ |

## 3.3 Domestic Hot Water System

The domestic hot water (DHW) system consists of a cold water (CW) intake, an accumulator and a circulation pump. The accumulator is a cuboid-shaped tank split vertically into four and connected in series, as shown in the P&ID (fig. 3.1). The flow through the DHW pipes is dependent on hot water consumption and whether the R744 heat pump (HP) is producing hot water. Any hot water consumption ($l/s$) larger than the R744 HP produces, will force a flow through the accumulator tanks, cooling the tanks from bottom left to top right. When the HP produces more hot water than is consumed, the flow through the accumulator tanks will be the other way around, filling hot water at the position of *RT301* and removing cold water at *RT314*.

## 3.4 Space Heating System

The space heating is distributed through floor heating pipes and therefore a low-temperature space heating system. The $CO_2$ HP works as a primary space heater, while the propane HP functions as a peak load heater, reheating the supply water when needed. The hydronic water is circulated with a circulation pump, and on/off valves control flow through each room based on heating demand.

## 3.5 Heat Sources

The heat sources consist of a ground heat source, an ambient heat source and a ventilation exhaust heat exchanger. After implementation of the ambient source, the brine will be directed either through the ambient heat source or the ground heat source based on the ambient temperature. The ventilation exhaust heat exchanger is connected in parallel with a hydronic resistance to direct only a portion of the flow through the heat exchanger to reduce pressure loss. Main ambient heat exchanger properties can be found in table 3.5. Further details are given in appendix A.2.

Table 3.5: Ambient heat source specifications[13]

| Model | GFVC FD 080.1/11-10 |
|---|---|
| Surface area | 62.2 $m^2$ |
| Dimensions | |
| Length | 1284 mm |
| Width | 608 mm |
| Height | 1153 mm |
| Circuits | 1N |
| Distributions | 5 |
| Tube material | Copper |
| Fin material | Aluminium |
| Fin spacing | 3.00 mm |

# 4 Method

This section introduces the software used to develop the model and visualise the data collected, both from models and existing heat pumping systems at hand. Then the model development of both the R744 and the R290 Dymola model is explained step by step before describing the validation process.

## 4.1 Software

### 4.1.1 CoolPack v1.5.0

CoolPack is a collection of refrigeration programs. It was first developed by the Department of Mechanical Engineering at the Technical University of Denmark (DTU) and has later been updated continuously.[14] The two programs used in this thesis are the CoolTools Cycle Analysis and Refrigeration Utilities. Cycle Analysis lets the user work with different steady state systems, like a one-stage transcritical cycle with $CO_2$, analysing the effects of changes in important variables. Refrigeration Utilities is an excellent tool for creating different diagrams, drawing refrigeration cycles and collecting state point data.

### 4.1.2 Modelica Programming Language and Dymola 2021

Dymola is a modelling software using the object-oriented programming language Modelica.[15] The interface works with a drag-and-drop method to a block diagram, as seen in the Dymola figures later presented in sections 4.2 and 4.3. Alongside the standard Modelica Library, the TIL Library was used to develop the models. The TIL Library includes models for components such as heat exchangers, compressors and expansion valves.

### 4.1.3 DaVE - Data Visualisation & Simulation Environment

DaVE is a data visualisation software, communicating well with the Dymola program. Dymola saves all simulation variables in a MATLAB file (filename.mat) which can be imported into DaVE. Refrigeration cycles can be visualised in diagrams as $\log p - h$ or $T - s$, and temperatures can be shown as a function of position in components like heat exchangers.

## 4.2 R290 Model in Dymola

The R290 Dymola model is based on data collected from the heat pump interface and visual inspection of the physical heat pump. Known data is compared to the Dymola simulation in section 5. This model was not built component-by-component as the R744 model. Instead, all components were added and then adjusted to reach the same conditions as observed at the site (fig. 4.1).

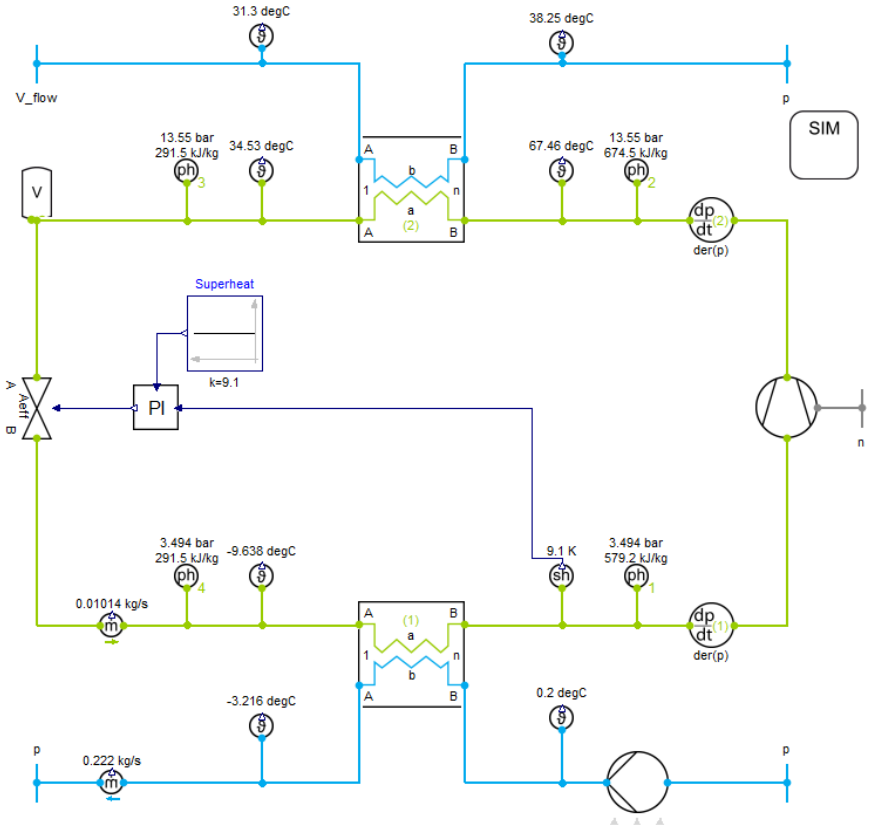


Figure 4.1: R290 model as shown in Dymola. The lower blue line shows brine through the evaporator, while the upper blue line shows hydronic flow through the condenser.

### 4.2.1 Evaporator and Ground Source

The evaporator was modelled as a plate heat exchanger. The brine inlet temperature was set to 0.2 °C with a volumetric flow of 770 l h$^{-1}$. Then the heat exchanger parameters were set to reach a superheating of 9.1 K.

Table 4.1: Evaporator input in Dymola. Tube a and b represents propane and brine tubes respectively.

| Variable | Propane | Brine | Wall |
|---|---|---|---|
| hx Geometry | | | |
| Number of plates | | | 10 |
| Length | | | 0.3 m |
| Width | | | 0.15 m |
| $\phi$ | | | 35° |
| Wall thickness | | | 0.7 mm |
| Pattern amplitude | | | 2 mm |
| Pattern wave length | | | 12.6 mm |
| Heat transfer model | Constant alpha | Constant alpha | |
| Constant alpha | 2000 W m$^{-2}$ K$^{-1}$ | 2000 W m$^{-2}$ K$^{-1}$ | |
| Pressure drop model | dp= 0 Pa | dp= 0 Pa | |
| Wall material | | | Stainless steel |
| Wall heat conduction model | | | Geometry based conduction |

### 4.2.2 Compressor

The compressor was designed to deliver approximately $0.01\,\mathrm{kg\,s^{-1}}$ at 9.1 K superheat and 4 bar suction pressure with a frequency of 60 Hz.

Table 4.2: Compressor and rotary boundary input in Dymola.

| Variable | |
|---|---|
| Compressor type | effCompressor |
| Use mechanical port | True |
| displacement | $2.8621 \times 10^{-5}\,\mathrm{m^3}$ |
| Compressor efficiencies | |
| Volumetric | 0.8 |
| Isentropic | 0.7 |
| Effective isentropic | 0.7 |
| Rotary boundary | |
| Boundary type | $n$ |
| Fixed $n$ | 60 Hz |

### 4.2.3 Condenser

The condenser is modelled similarly to the evaporator; size and heat resistance is set to achieve the same hydronic conditions as observed. Hydronic flow is set to $483\,\mathrm{l\,h^{-1}}$ and return temperature to 31.3 °C. Then the heat exchange parameters were modified to reach a supply temperature of 38.3 °C.

Table 4.3: Condenser input in Dymola. Tube a and b represents propane and brine tubes respectively.

| Variable | Propane | Brine | Wall |
|---|---|---|---|
| hx Geometry | | | |
| Number of plates | | | 15 |
| Length | | | 0.3 m |
| Width | | | 0.15 m |
| $\phi$ | | | 35° |
| Wall thickness | | | 0.75 mm |
| Pattern amplitude | | | 2.00 mm |
| Pattern wave length | | | 12.60 mm |
| Heat transfer model | Constant alpha | Constant alpha | |
| Constant alpha | $2500\,\mathrm{W\,m^{-2}\,K^{-1}}$ | $2500\,\mathrm{W\,m^{-2}\,K^{-1}}$ | |
| Pressure drop model | dp= 0 Pa | dp= 0 Pa | |
| Wall material | | | Stainless steel |
| Wall heat conduction model | | | Geometry based conduction |

### 4.2.4 Expansion Valve

The expansion valve varies flow with an effective flow area controlled by the PI controller. The PI controller adjusts the flow area to achieve a given superheat at the evaporator outlet.

Table 4.4: Expansion valve and controller input in Dymola.

| Variable | |
|---|---|
| Expansion valve | |
| Valve flow variable type | Effective flow area |
| Use effective flow area input | True |
| Controller | |
| Controller type | PI |
| Invert feedback | False |
| Integral parameter type | $T_i$ |
| $k$ | $5 \times 10^{-9}$ |
| $T_i$ | 10 s |
| $y_{max}$ | $2 \times 10^{-5}$ |
| $y_{min}$ | $8 \times 10^{-9}$ |
| $y_{initial}$ | $3 \times 10^{-7}$ |
| Superheat setpoint | 9.1 K |

## 4.3 R744 Model in Dymola

This part explains the step by step development of the R744 model in Dymola. The order of steps follows the order of subsections. The components were added to each other until the circuit was complete and a closed loop, starting with the evaporator and following the direction of refrigerant flow. In addition to the data listed in the following tables, initialisation data was added to increase the simulation speed.

### 4.3.1 Evaporator and Heat Sources

First off, the evaporator was modelled with given geometric data and steady-state conditions collected with the heat pump in operation. Refrigerant mass flow, pressure, inlet and outlet state points were known, as well as brine inlet temperature. As the geometry is given, the overall heat transfer resistance was modified to obtain the same results as the $CO_2$ heat pump at multiple steady states. A heat transfer coefficient best matching all steady states was chosen.

**The ground heat source** is modelled in the brine loop as a tube with a heat port. The heat port has a heat resistance of $1 \times 10^{-3}\,\mathrm{K\,W^{-1}}$, and is connected to a series of three heat resistances and two heat capacitors before reaching the heat boundary with a constant temperature of 7.5 °C. Starting from the heat boundary, the resistances are $1/2250\,\mathrm{K\,W^{-1}}$, $1/1750\,\mathrm{K\,W^{-1}}$ and $1/1175\,\mathrm{K\,W^{-1}}$ and the heat capacities are

Table 4.5: Evaporator input in Dymola. Tube a and b represents $CO_2$ and brine tubes respectively.

| Variable | Tube a, $CO_2$ | Tube b, brine | Wall |
|---|---|---|---|
| hx Geometry | | | |
| Tube length | 12 m | 12 m | |
| Inner diameter | 8 mm | 20 mm | |
| Heat transfer model | Evaporation: constant alpha, 1-phase: Gnielinski Dittus Boelter | Constant alpha | |
| alpha two phase | $1575\,\mathrm{W\,m^{-2}\,K^{-1}}$ | | |
| correction factor | 1 | | |
| constant alpha | | $2500\,\mathrm{W\,m^{-2}\,K^{-1}}$ | |
| Pressure drop model | $dp = 0\,\mathrm{Pa}$ | Constant pressure drop $dp = 20\,\mathrm{kPa}$ | |
| Thermal Resistance | | | $3.5 \times 10^{-4}\,\mathrm{K\,W^{-1}}$ |

$10 \times 10^9\,\mathrm{J\,K^{-1}}$ and $1 \times 10^9\,\mathrm{J\,K^{-1}}$. The heat resistances and capacitors are designed to reach the same results as observed in multiple steady state cases. The tube is set to have a constant pressure loss of 100 kPa. A circulation pump forces the brine with a pump efficiency of $\eta = 0.4$ and drive efficiency, $\eta_{drive} = 1.0$. The pump is imported from the TIL library.

**The ambient heat source** is modelled as a fin and tube heat exchanger with crossflow, imported from the TIL library and modified to replicate the heat exchanger provided by Güntner. Model details can be found in table 4.6 and data given by Güntner in Appendix A.2.

Table 4.6: Ambient heat exchanger input in Dymola.

| Variable | |
|---|---|
| hx Geometry | |
| Finned tube length | 1150 mm |
| Number of serial tubes | 2 |
| Serial tube distance | 121 mm |
| Number of parallel tubes | 12 |
| Liquid | |
| Constant pressure drop | 20 kPa |
| Constant alpha | $2500\,\mathrm{W\,m^{-2}\,K^{-1}}$ |
| Tube | |
| Wall material | Copper |
| Wall conduction model | Geometry based conduction |
| Fin | |
| Wall material | Aluminium |
| Fin efficiency | 1-D approximation (Schmidt) |
| Moist air | |
| Fin side heat transfer model | Haaf, correction factor =1.4 |
| Fin side pressure drop model | Zero pressure drop |

The ambient heat source fan is not modelled and its power demand is therefore not included in the total performance calculations. The data sheet provided states a power consumption of 0.02 kW at the boundary conditions used in this project (appendix A.2). [13]

**The R290 evaporator** was later added as a tube with a heat port. The heat absorbed through the R290 evaporator is set to be two thirds of the heat delivered through the condenser. As the heat transfer is given by input, the tube heat resistance is insignificant. The pressure drop through the evaporator is set to 10 kPa.

### 4.3.2 Compressor and Low Pressure Receiver

After tuning the evaporator to behave as in the observed steady-state, the low pressure receiver was added to the system, following the evaporator.

Table 4.7: Low pressure receiver input in Dymola.

| Variable | |
|---|---|
| Volume | $10 \times 10^{-3}\,\mathrm{m}^3$ |
| Initial filling level | 0.20 |

The efficiency-based compressor was added from the TIL library and controlled by a rotary boundary with input. An ambient temperature dependant equation output then controlled the compressor frequency.

Table 4.8: Compressor input in Dymola.

| Variable | |
|---|---|
| Compressor type | effCompressor |
| use mechanical port | true |
| displacement | $4.614\,956\,777 \times 10^{-6}\,\mathrm{m}^3$ |
| Compressor efficiencies | |
| Volumetric | 0.8 |
| Isentropic | 0.633 925 |
| Effective isentropic | 0.7 |

### 4.3.3 Gas Coolers and Heat Sinks

The tripartite gas cooler configuration was added, together with the heat sinks, domestic hot water heating and hydronic space heating. The geometric data was given, and the heat transfer resistance was adjusted to obtain results as steady-state conditions observed at the site. Following the compressor, the refrigerant entered the reheating gas cooler (GC1) first, with the function to lift the remaining domestic hot water temperature to about 70 °C. To accomplish this, the DHW inlet mass flow boundary was controlled by a PI controller set to maintain 70 °C at GC1 outlet. Later, in all case simulations, the PI controller was removed, and domestic hot water mass flow was set to the same as observed at the site.

Table 4.9: DHW reheat gas cooler input in Dymola. Tube a and b represents $CO_2$ and DHW tubes, respectively.

| Variable | Tube a, $CO_2$ | Tube b, DHW | Wall |
|---|---|---|---|
| hx Geometry | | | |
| Tube length | 3.5 m | 3.5 m | |
| Inner diameter | 6 mm | 12 mm | |
| Heat transfer model | Constant alpha | Gnielinski Dittus Boelter | |
| correction factor | | 10 | |
| constant alpha | $1750\,\mathrm{W\,m^{-2}\,K^{-1}}$ | | |
| Pressure drop model | $dp = 0\,\mathrm{Pa}$ | $dp = 0\,\mathrm{Pa}$ | |
| Thermal Resistance | | | $5 \times 10^{-4}\,\mathrm{K\,W^{-1}}$ |

The refrigerant then entered the space heating gas cooler (GC2), heating the hydronic water cooled by the ambient. The hydronic water circulated with a mass flow of $0.134\,\mathrm{kg\,s^{-1}}$ and had an accumulator tank with a volume of 200 l. The R290 heat pump was modelled to adequately heat the supply water when this was too cold over a period of time. The heat sinks and controls are further explained in section 4.3.7.

Table 4.10: Space heating gas cooler input in Dymola. Tube a and b represents $CO_2$ and hydronic tubes respectively.

| Variable | Tube a, $CO_2$ | Tube b, hydronic | Wall |
|---|---|---|---|
| hx Geometry | | | |
| Tube length | 15 m | 15 m | |
| Inner diameter | 6 mm | 18 mm | |
| Heat transfer model | Constant alpha | Gnielinski Dittus Boelter | |
| correction factor | | 1 | |
| constant alpha | $1750\,\mathrm{W\,m^{-2}\,K^{-1}}$ | | |
| Pressure drop model | $dp = 0\,\mathrm{Pa}$ | $dp = 20\,\mathrm{kPa}$ | |
| Thermal Resistance | | | $5 \times 10^{-4}\,\mathrm{K\,W^{-1}}$ |

The heat sink and R290 condenser were modelled as tubes with heat flow boundaries and a pressure drop of 20 kPa and 10 kPa, respectively. Hydronic pump input is presented in table 4.11.

Table 4.11: Hydronic pump input in Dymola.

| Variable | |
|---|---|
| Component name | JP001 |
| Pump efficiency | 0.4 |
| Drive efficiency | 1.0 |
| Mass flow | $0.134\,\mathrm{kg\,s^{-1}}$ |

Lastly, the refrigerant entered the DHW preheating gas cooler (GC3), lowering the $CO_2$ temperature to a minimum and lifting the water temperature (tab. 4.12).

Pressure loss was neglected in the heat exchangers to simplify the model and increase simulation speed.

Table 4.12: DHW preheat gas cooler input in Dymola. Tube a and b represents $CO_2$ and DHW tubes respectively.

| Variable | Tube a, $CO_2$ | Tube b, DHW | Wall |
|---|---|---|---|
| hx Geometry | | | |
| Tube length | 14 m | 14 m | |
| Inner diameter | 6 mm | 12 mm | |
| Heat transfer model | Constant alpha | Gnielinski Dittus Boelter | |
| correction factor | | 3 | |
| constant alpha | $1750\,\mathrm{W\,m^{-2}\,K^{-1}}$ | | |
| Pressure drop model | $dp = 0\,\mathrm{Pa}$ | $dp = 0\,\mathrm{Pa}$ | |
| Thermal Resistance | | | $5.0 \times 10^{-4}\,\mathrm{K\,W^{-1}}$ |

The three-way directional valve *SC001* was implemented to direct the cold water past the preheating gas cooler whenever the water had a higher temperature than the $CO_2$ at the inlets; *If RT011.sensorValue > RT005.sensorValue then 1 else 0.*

### 4.3.4 Expansion Valve and Suction Gas Heat Exchanger

The suction gas heat exchanger is modelled as a Tube-and-Tube heat exchanger with parallel flow and geometry as described by Stene [12].

Table 4.13: Suction gas heat exchanger input in Dymola. Tube a and b represents suction side and high pressure side, respectively.

| Variable | Tube a | Tube b | Wall |
|---|---|---|---|
| hx Geometry | | | |
| Tube length | 2.3 m | 2.3 m | |
| Inner diameter | 8 mm | 12 mm | |
| Heat transfer model | Constant alpha | Constant alpha | |
| Constant alpha | $3000\,\mathrm{W\,m^{-2}\,K^{-1}}$ | $3000\,\mathrm{W\,m^{-2}\,K^{-1}}$ | |
| Pressure drop model | $dp = 0\,\mathrm{Pa}$ | Konakov correlation for smooth pipes | |
| Thermal Resistance | | | $3 \times 10^{-4}\,\mathrm{K\,W^{-1}}$ |

Next, the expansion valve with a controller was added. The expansion valve is given an effective flow area input by the PI controller working to achieve a high pressure setpoint.

[i] Proportional gain
[ii] Time constant of integrator block

Table 4.14: Expansion valve and controller input in Dymola.

| Variable | |
|---|---|
| Expansion valve | |
| Valve flow variable type | Effective flow area |
| Use effective flow area input | True |
| Controller | |
| Controller type | PI |
| Invert feedback | True |
| $k^{\mathrm{i}}$ | $2 \times 10^{-9}$ |
| $T_i^{\mathrm{ii}}$ | $1 \times 10^{-1}\,\mathrm{s}$ |
| $y_{max}$ | $1 \times 10^{-6}$ |
| $y_{min}$ | $4 \times 10^{-8}$ |
| $y_{initial}$ | $9 \times 10^{-8}$ |
| Activation time | 10 s |

To achieve the desired compressor inlet superheat, as observed at site, a portion of the fluid was set to bypass the suction gas heat exchanger. This was accomplished with a directional valve (tab. 4.15).

Table 4.15: Directional valve input in Dymola.

| Variable | |
|---|---|
| Switching position fixed | 0.63 |
| Effective Flow $\mathrm{Area}_0$ | $1 \times 10^{-5}\,\mathrm{m}^2$ |
| Effective Flow $\mathrm{Area}_1$ | $1 \times 10^{-5}\,\mathrm{m}^2$ |

### 4.3.5 Subcooler

As the subcooler is built as a pipe coiled around another pipe, it is modelled as two tubes with a heat resistance (fig. 4.2). This is done by enabling heat ports on each tube and setting the heat resistance at each port (tab. 4.16).

Table 4.16: Subcooler input in Dymola. Tube a and b represents $CO_2$ and brine tubes respectively.

| Variable | Tube a, $CO_2$ | Tube b, brine |
|---|---|---|
| hx Geometry | | |
| Tube length | 10 m | 0.5 m |
| Inner diameter | 6 mm | 18 mm |
| Tube side heat transfer model | Constant alpha | Constant alpha |
| Constant alpha | $3000\,\mathrm{W\,m^{-2}\,K^{-1}}$ | $1000\,\mathrm{W\,m^{-2}\,K^{-1}}$ |
| Pressure drop model | $dp = 0\,\mathrm{Pa}$ | $dp = 5\,\mathrm{kPa}$ |
| Wall heat conduction model | Constant wall heat resistance | Constant wall heat resistance |
| Constant resistance | $8 \times 10^{-3}\,\mathrm{K\,W^{-1}}$ | $8 \times 10^{-3}\,\mathrm{K\,W^{-1}}$ |
| Wall material | Stainless steel | Stainless steel |

### 4.3.6 Closed Loop

With the fluid state at the outlet reaching somewhat the same condition as the inlet, the loop was closed, and a complete cycle was achieved. After closing the loop, many changes have been made to further improve the model. The parameters given in this chapter are from the final result.

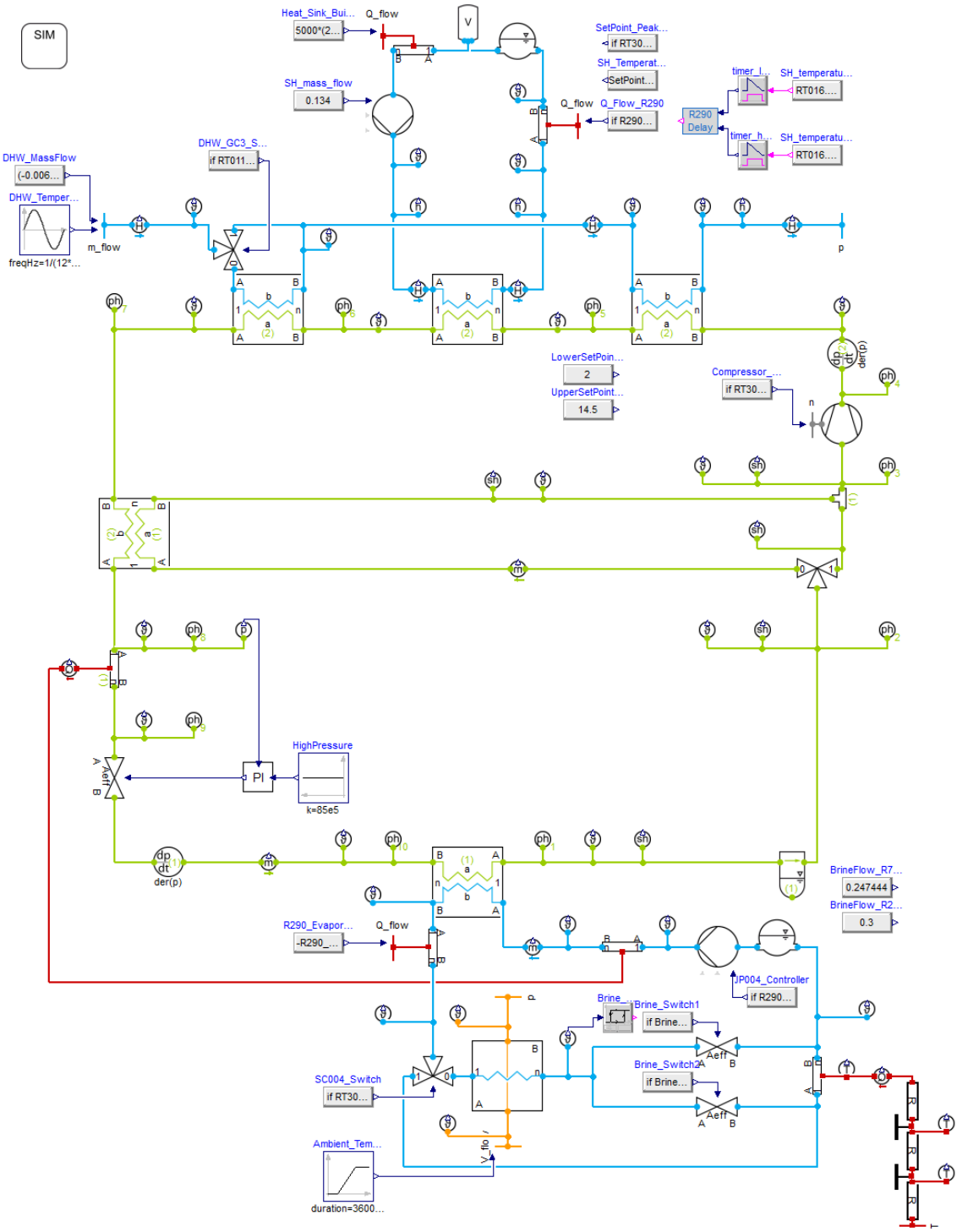


Figure 4.2: R744 model as shown in Dymola.

### 4.3.7 Heat Pump Controls

This section describes the controls found in the R744 Dymola model. These controls are made similar to controls designed for implementation in the heat pump system. Various model inputs are listed in table 4.17.

Table 4.17: Model input, unless simulation specific inputs are stated.

| Parameter | Input |
|---|---|
| Brine flow | |
| When R744 is running | $0.247\,444\,\mathrm{kg\,s^{-1}}$ |
| When R744 and R290 is running | $0.6\,\mathrm{kg\,s^{-1}}$ |
| Ground heat source temperature | 7.5 °C |
| High pressure | 85 bar |
| Space heating demand at −20 °C ambient | 5 kW |
| DHW cold water inlet temperature | 15 °C |
| DHW cold water mass flow | $6.4575 \times 10^{-3}\,\mathrm{kg\,s^{-1}}$ |
| Hydronic mass flow | $0.134\,\mathrm{kg\,s^{-1}}$ |
| Hydronic supply temperature setpoint | |
| For ambient temperature $\leq -15$ °C | 35 °C |
| For ambient temperature $\geq 15$ °C | 28 °C |
| For ambient temperature $(-15, 15)$°C | Linear decrease from 35 °C to 28 °C |
| Compressor frequency | |
| For ambient temperature $\leq 2$ °C | 60 Hz |
| For ambient temperature $\geq 14.5$ °C | 30 Hz |
| For ambient temperature $(2, 14.5)$°C | Linear increase from 30 Hz to 60 Hz |
| SC004_Switch setpoint | 2 °C |

**The Heat Source** is either ambient only, ground only or a combination of these two. This is solved with one three-way directional valve and two orifice valves (fig. 4.2). Exiting the evaporator, the brine enters *SC004*, which directs the brine to the ambient heat source if the ambient temperature is above setpoint. If the ambient temperature is below setpoint, the brine only circulates through the ground heat source. When the ambient temperature is above setpoint, and the brine has exited the ambient heat source, the brine temperature is measured. A hysteresis was implemented to determine whether the brine continues through the ground heat source or directly to the evaporator again (tab. 4.18). The brine will therefore be directed through the ground heat source when the brine temperature is below 4.0 °C and to the evaporator when above 5.2 °C.

Table 4.18: Brine switch hysteresis

| Variable | |
|---|---|
| $\mathrm{u}_{low}$ | 4.0 |
| $\mathrm{u}_{high}$ | 5.2 |
| $\mathrm{pre}_{y,\,start}$ | True |

The brine pump, *JP004*, has two mass flow setpoints, one for when the R744 heat pump is running and one for when both heat pumps are running.

**The Compressor** is controlled by a linear ambient temperature dependant equation between two setpoints. When the ambient temperature is below the lower setpoint, the frequency is set to 60 Hz; when higher than the upper setpoint, the frequency is 30 Hz. Between these two setpoints, the frequency has a linear increase.

**The Heat Sinks** are domestic hot water and space heating. The space heating demand is ambient temperature dependant, with a demand of 5 kW at an ambient temperature of −20 °C, 0 kW at 21 °C and a linear increase between these two points. The R290 condenser was modelled as a tube with a heat port, controlled by a delay and hysteresis, constructed to engage the R290 heat pump when supply temperature stayed below setpoint for more than one hour and deactivate when above setpoint for more than two hours. The supply temperature setpoint was 35 °C for ambient temperatures below −15 °C, 28 °C for ambient temperatures above 15 °C and linear between these two points. When engaged, the R290 condenser delivered sufficient heat to maintain a supply temperature at setpoint. To simplify the model, the thermal inertia of the system was neglected past the volume of 200 l, and the R290 heat pump was given a minimum heating capacity of 500 W.

### 4.3.8 Validation Process

First, the model was validated using one steady state scenario. The model was modified until performing adequately, component by component and as a system. Later each comparable component was given boundary conditions as observed in selected steady state scenarios ($n = 11$), including different heat modes; high and low pressures. The main components were comparable with inlet and outlet conditions at steady state:

- Evaporator
- Compressor
- Preheating gas cooler
- Space heating gas cooler
- Reheating gas cooler

To test and validate each component, the components were duplicated and exposed to boundary conditions for selected steady states representing different situations (fig. 4.3). Once all components behaved as needed, the component inputs were evaluated, and a set of inputs were chosen to represent this component. Then the component was tested in all known steady state situations to verify satisfactory performance. The original steady state data is shown in appendix A.1.

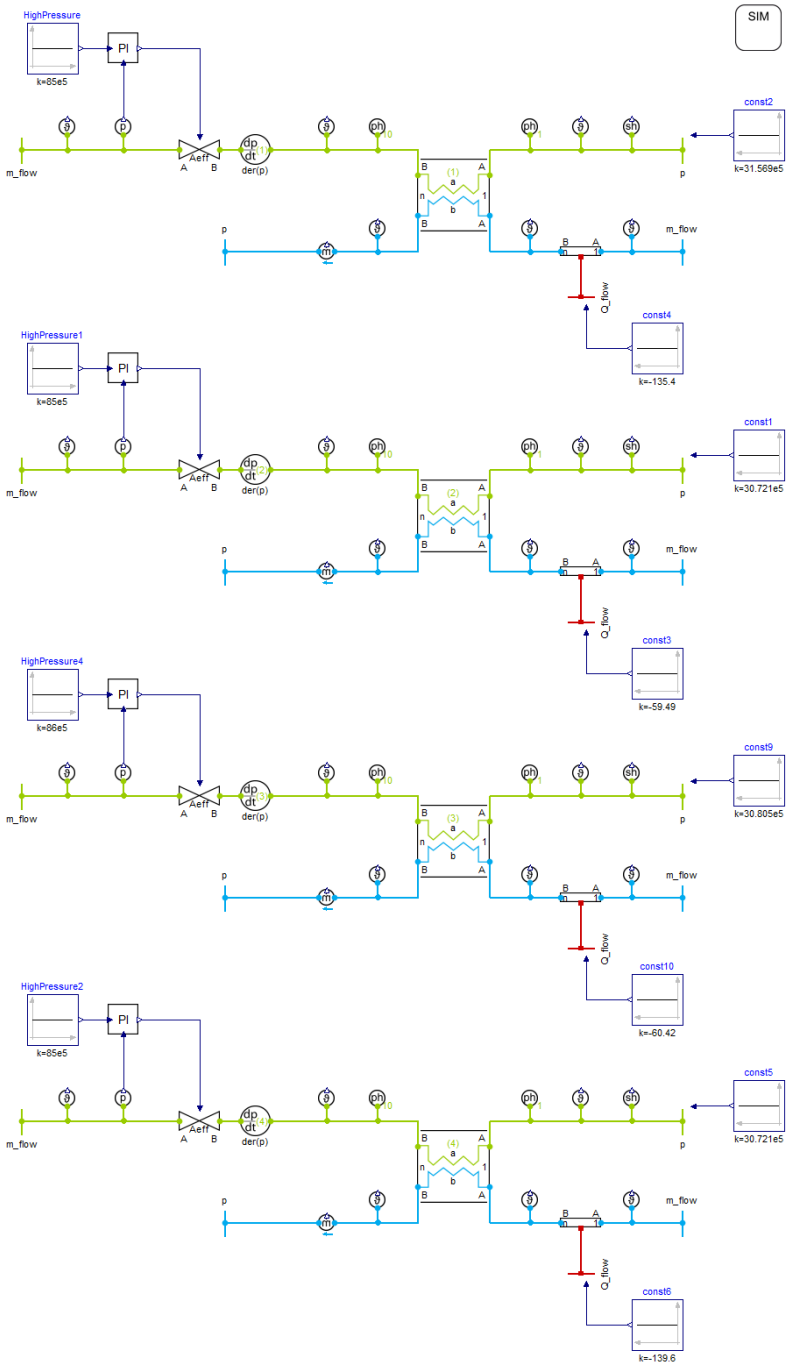


Figure 4.3: The process of testing and validating the evaporator in multiple steady state scenarios. Each evaporator is tested under different boundary conditions.

## 4.4 R744 Dymola Simulation Campaign

To evaluate the effect of various parameters, changes were split into different cases, varying only one or few parameters at a time. This is done to efficiently identify which parameter changes are most effective. The following subsections describe which changes were made to the model preceding and during each simulation. First off, the simulations were given a ten-hour initialisation period, to ensure steady state. Then the changes were made over a period of five days, usually with a ramp.

### 4.4.1 Case 1: Ambient Temperature and Heat Source Variation

In this case, simulations were done in three modes; ground source only, ambient heat source only and combined heat source. This was done by manipulating the flow through the three- and two-way valves. The code in *SC004 Switch* gives input to the three-way valve *SC004* on whether to include the ambient heat source by comparing its setpoint and the ambient temperature (fig. 4.2). The setpoint was adjusted to force flow as fitting for each simulation.

*if RT307.sensorValue < [Setpoint] then 1 else 0.*

The two-way valves are controlled by the brine temperature exiting the water-air heat exchanger. In the simulation with only the ambient heat source, the two-way valves were forced open and closed to direct the flow past the ground heat source.

The simulations were conducted with a constant DHW flow and inlet temperature of 15 °C, an ambient temperature dependant space heating demand varying from 5 kW to 0 kW and an R290 peak load heat pump controlled by the hydronic supply and ambient temperature. The simulation is initialised at an ambient temperature of −20 °C before the ambient temperature is increased with a ramp from −20 °C to 20 °C over a period of five days.

- Simulation 1.01: combined heat source
- Simulation 1.02: ambient heat source
- Simulation 1.03: ground heat source

### 4.4.2 Case 2: Cold Water Temperature Variation

The cold water temperature entering the preheating gas cooler (GC3) is increased with a ramp from 5 °C to 40 °C over a period of five days. As an initialisation, the cold water held a temperature of 5 °C for ten hours before the ramp increase. Eight simulations were conducted to see the effect in different situations. Firstly four simulations were done with only changes to the ambient temperature, which in turn also changes both space heating demand and compressor frequency (tab. 4.19). The last four simulations were conducted in DHW-mode, only heating tap water, in four compressor frequency stages. The compressor frequency was forced as it usually is dependent on ambient temperature.

Table 4.19: Case 2 specific input.

| Parameter | Simulation | | | | | | | |
|---|---|---|---|---|---|---|---|---|
| | 2.01 | 2.02 | 2.03 | 2.04 | 2.05 | 2.06 | 2.07 | 2.08 |
| Ambient temperature | −15°C | −5°C | 5°C | 15°C | 5°C | 5°C | 5°C | 5°C |
| Space heating demand | | | | | 0 kW | 0 kW | 0 kW | 0 kW |
| Compressor frequency | | | | | 30 Hz | 40 Hz | 50 Hz | 60 Hz |

### 4.4.3 Case 3: High Pressure Variation

In case 3 the high pressure is varied from 78 bar to 100 bar in ten simulations. Four simulations were done with ambient temperatures from −15 °C to 15 °C. Four with a cold water inlet temperature from 5 °C to 30 °C and one in each heat mode with 5 °C cold water.

Table 4.20: Case 3 specific input.

| Simulation | Ambient temperature | Heat mode | Cold water inlet temperature |
|---|---|---|---|
| 3.01 | −15 °C | Combination | 5 °C |
| 3.02 | −5 °C | Combination | 5 °C |
| 3.03 | 5 °C | Combination | 5 °C |
| 3.04 | 15 °C | Combination | 5 °C |
| 3.05 | 5 °C | DHW ($f = 30$ Hz) | 5 °C |
| 3.06 | 5 °C | Space | 5 °C |
| 3.07 | 5 °C | Combination | 10 °C |
| 3.08 | 5 °C | Combination | 20 °C |
| 3.09 | 5 °C | Combination | 30 °C |

### 4.4.4 Case 4: Brine Temperature Variation

Case 4 varies the brine temperature through four simulations in different heat modes: domestic hot water (DHW) heating only, space heating only and a combination of DHW and space heating. After ten hours of initialisation with constant boundaries, the brine temperature is increased with a ramp from −5 °C to 15 °C over a period of five days. In combination mode the compressor frequency is given by the ambient temperature ($T_{amb} = 5$ °C), while in DHW and space heating mode it is set to 30 Hz.

Table 4.21: Case 4 specific input.

| Simulation | Heat mode | Compressor frequency |
|---|---|---|
| 4.01 | Combination | 52.8 Hz |
| 4.02 | Space heating | 30.0 Hz |
| 4.03 | DHW | 30.0 Hz |

### 4.4.5 Case 5: Hydronic Return Temperature Variation

The hydronic water temperature returning to the space heating gas cooler is varied with a ramp from 20 °C to 60 °C over a period of five days. This is done in two simulations: combination mode and space heating mode. The ambient temperature is set to 15 °C, and as a result, the compressor frequency is 30 Hz. During the simulations, the R290 peak load heat pump is switched off.

Table 4.22: Case 5 specific input.

| Simulation | Heat mode |
|---|---|
| 5.01 | Combination |
| 5.02 | Space heating |

### 4.4.6 Case 6: Brine Flow Variation

The brine flow was varied from $0.05\,\mathrm{kg\,s^{-1}}$ to $0.50\,\mathrm{kg\,s^{-1}}$ over a period of five days while all other parameters are kept constant. Ambient temperature is set to 5 °C, and cold water enters the preheating gas cooler with a temperature of 10 °C. The heat transfer coefficient is kept constant as in all other simulations, while pressure drop in brine through components follows either a quadratic mass flow dependant calculation or Konakovs correlation for smooth pipes (tab. 4.23).

Table 4.23: Case 6 specific pressure drop in brine circuit.

| Component | Pressure drop model | Model specifications |
|---|---|---|
| R744 Evaporator | Quadratic mass flow dependant | $\dot{m}_{nom} = 0.225\,\mathrm{kg\,s^{-1}}$ $\Delta p_{nom} = 18\,\mathrm{kPa}$ |
| R290 Evaporator | Konakov correlation for smooth pipes | Correction factor = 1 |
| Liquid/air heat exchanger | Quadratic mass flow dependant | $\dot{m}_{nom} = 0.225\,\mathrm{kg\,s^{-1}}$ $\Delta p_{nom} = 18\,\mathrm{kPa}$ |
| Ground heat exchanger | Konakov correlation for smooth pipes | Correction factor = 1 |
| Sub cooler | Konakov correlation for smooth pipes | Correction factor = 1 |

Three simulations were conducted, one for each heat mode: combination, space heating and DHW mode.

# 5 Results

This chapter will first present results from the process of validating the Dymola Modelica models. Next, the results of the simulation campaign are presented case by case.

## 5.1 Dymola Modelica Model Validity

This section will present comparative data from the physical heat pumps and Dymola simulations in order to validate the models. The models are compared to steady state data from the heat pumps.

### 5.1.1 Validity of R744 Dymola Modelica Model

The model was first constructed and compared to a single steady state case; this will be presented in detail in the following. Later, as each component was adjusted to behave as and compared to several steady state cases, the compared temperatures, heat flows and pressures in the Dymola model gave no deviations above 5 % and few above 2 %.

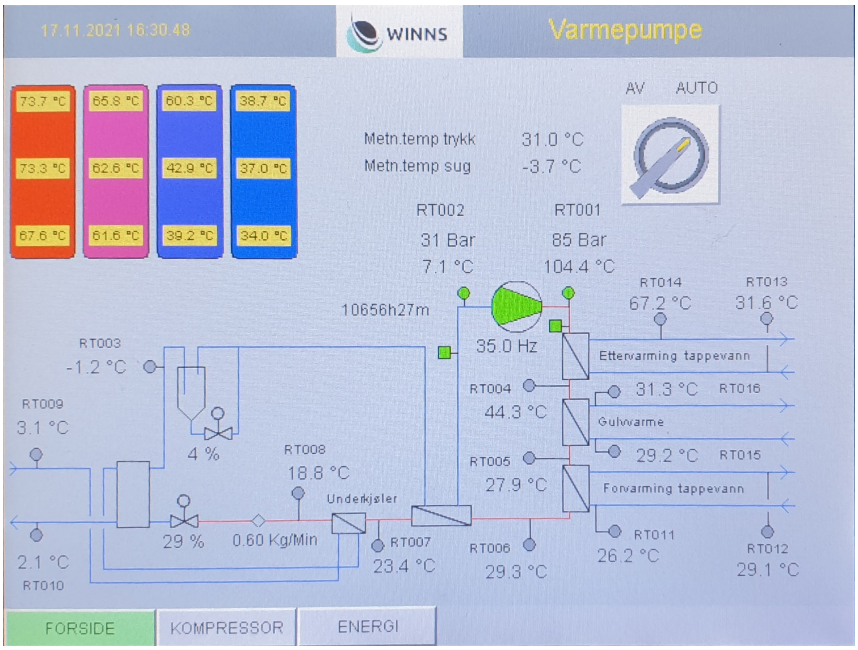


Figure 5.1: Picture of R744 heat pump display at steady state conditions, heating hydronic and reheating domestic hot water.

To validate the Dymola model at a steady state, parameters were compared to known values given by the R744 heat pump interface (fig. 5.1). This is a case with high DHW temperature at tri-partite gas cooler inlet, providing little heat transfer in the preheat gas cooler (fig. 5.3a). This is seen both in the model and the physical heat pump. Worth noticing is that the temperatures given by $RT005$ and $RT006$ indicate a heat flow from the DHW to the $CO_2$. This is due to the significant uncertainty in the $CO_2$ temperature sensors (fig. 5.1).

The results show overall minor deviations from the steady state condition achieved by the heat pump. Most of the most considerable deviations are closely related to the compressor: mass flow, compressor outlet state, and frequency. All comparable data collected is shown in table 5.1.

Table 5.1: Steady state comparison of Dymola model and heat pump unit at site.

| Parameter | Dymola model | Heat pump unit | | Deviation |
|---|---|---|---|---|
| COP | 4.0 | | | |
| Compressor frequency | 40[i] | 35 | Hz | 14% |
| Specific heating capacity, $h_{GC,inlet} - h_{GC,outlet}$ | 239 | 245 | $\mathrm{kJ\,kg^{-1}}$ | −2.4 % |
| Refrigerant mass flow | 0.0106 | 0.0100 | $\mathrm{kg\,s^{-1}}$ | 6 % |
| Heating power | 2.53 | 2.45 | kW | 3.3 % |
| Low pressure | 33 | 31 | bar | 6.5 % |
| High pressure | 85[ii] | 85 | bar | 0.0 % |
| Refrigerant temperatures | | | | |
| Evaporator outlet | -2.0 | -1.2 | °C | −0.3 % |
| Compressor inlet | 7.5 | 7.1 | °C | 0.1 % |
| Compressor outlet | 93.5 | 104.4 | °C | −2.9 % |
| Reheating gas cooler outlet | 41.3 | 44.3 | °C | −0.9 % |
| Space heating gas cooler outlet | 29.2 | 29.3 | °C | 0.0 % |
| Preheating gas cooler outlet | 29.1 | 27.9 | °C | 0.4 % |
| SGHE outlet | 22.5 | 23.4 | °C | −0.3 % |
| Subcooler outlet | 17.2 | 18.8 | °C | −0.5 % |
| Brine temperatures | | | | |
| Return | 3.1[i] | 3.1 | °C | 0.0 % |
| Supply | 1.1 | 2.1 | °C | −0.4 % |
| DHW temperatures | | | | |
| Inlet preheating | 26.2[i] | 26.2 | °C | 0.0 % |
| Inlet reheating | 28.8 | 31.6 | °C | −0.9 % |
| Outlet reheating | 67.2[ii] | 67.2 | °C | 0.0 % |
| Space heating temperatures | | | | |
| Hydronic return | 29.2[i] | 29.2 | °C | 0.0 % |
| Hydronic supply | 31.4[ii] | 31.3 | °C | 0.0 % |

The resulting steady state cycle reached in the Dymola model is shown in a pressure-enthalpy and temperature-entropy diagram (fig. 5.2).

The amount of specific heat transported through each heat exchanger can also be seen visualised as horizontal lengths in the heat rejection section of the $\log p - h$ diagram (fig. 5.2a). The isotherms show a more rapid temperature reduction in the reheating gas cooler and slow condensation-like heat rejection in the space heating gas cooler. The water inlet temperature limits the heat rejection through the preheating gas cooler.

[i] Input
[ii] PI controlled

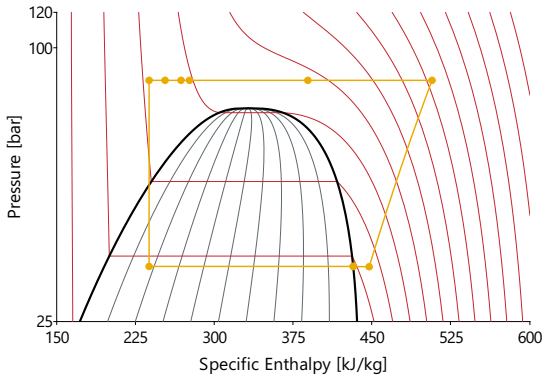


(a) Heat pump cycle in a logarithmic pressure - enthalpy diagram with red isotherms and grey lines showing constant steam quality.

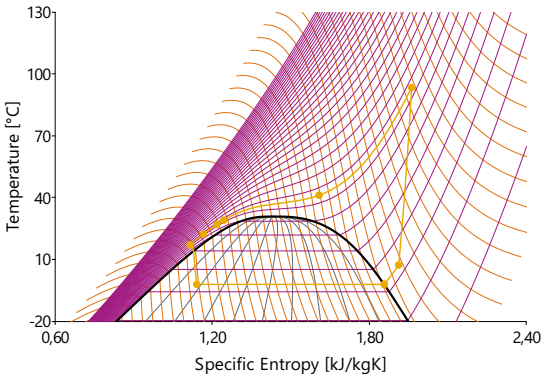


(b) Heat pump cycle in a temperature entropy diagram with isobars in violet, constant enthalpy lines in orange and steam quality in grey.

Figure 5.2: Achieved cycle in Dymola with steady state conditions. High pressure is 85 bar and low pressure is 33 bar.

The heat exchange through the tri-partite gas cooler is mainly in the reheating gas cooler and the space heating gas cooler. (fig. 5.3). In the space heating gas cooler, most heat exchange happens in half of the gas cooler (fig. 5.3b).

Each heat exchanger is divided into several cells where parameters, including temperature, are calculated at each cell. These cells are enumerated along the horizontal axis of the heat exchange figures (fig. 5.3 and 5.5).

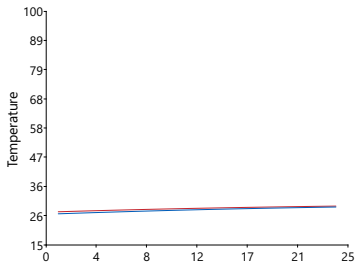


(a) Temperature distribution through DHW preheating gas cooler.

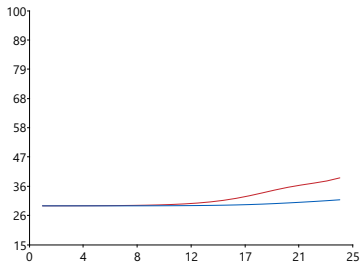


(b) Temperature distribution through space heating gas cooler.

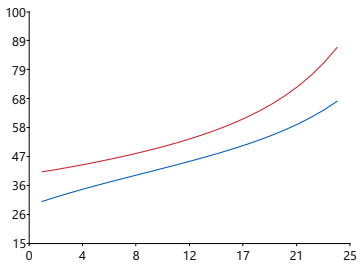


(c) Temperature distribution through DHW reheating gas cooler.

Figure 5.3: The red line shows R744 temperature distribution through each heat exchanger, and the blue line shows hydronic and DHW temperatures. The vertical axis shows temperature (°C), and the horizontal axis shows position by cell number. Cell number 1 refers to the water inlet, and cell number 24 refers to the water outlet in each gas cooler.

Following this, the main components were tweaked, improved and compared to multiple steady state scenarios ($n = 11$), giving no deviation above 5 % and few above 2 % in any of the compared temperatures, heat flows and pressures.

### 5.1.2 Validity of R290 Dymola Modelica Model

The R290 Dymola model is compared to parameters collected from the heat pump interface and energy meters at steady state conditions (tab. 5.2). The Dymola model delivers about the same amount of heat but works with a higher condensing pressure. Brine and hydronic flow and return temperatures are controlled parameters, giving no deviation.

Table 5.2: Steady state parameters of R290 Dymola model and heat pump unit at site.

| Parameter | Dymola model | Heat pump unit | | Deviation |
|---|---|---|---|---|
| COP | 3.2 | | | |
| Heating power | 3.88 | 3.7 | kW | 4.9 % |
| Cooling power | 2.51 | | kW | |
| Refrigerant flow | 0.010 | | $\mathrm{kg\,s^{-1}}$ | |
| Superheat | 9.1[iii] | 9.1 | K | |
| Evaporating pressure | 3.49 | | bar | |
| Condensing pressure | 13.55 | 12.3 | bar | 10.2 % |
| Brine flow | 770[iv] | 770 | $\mathrm{l\,h^{-1}}$ | |
| Brine temperatures | | | | |
| Return | 0.20[ii] | 0.2 | °C | |
| Supply | −3.22 | −3.0 | °C | |
| Hydronic flow | 484[ii] | 484 | $\mathrm{l\,h^{-1}}$ | |
| Space heating temperatures | | | | |
| Hydronic return | 31.30[ii] | 31.3 | °C | |
| Hydronic supply | 38.25 | 38.3 | °C | |

The model results acquired at steady state are visualised in a pressure - enthalpy diagram and a temperature - entropy diagram (fig. 5.4). The graphs show a well-functioning heat pump cycle with a large portion of heat collected from the heat source.

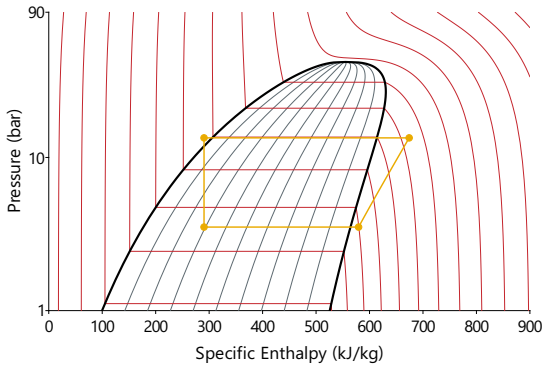


(a) Heat pump cycle in a logarithmic pressure - enthalpy diagram with red isotherms and grey lines showing constant steam quality.

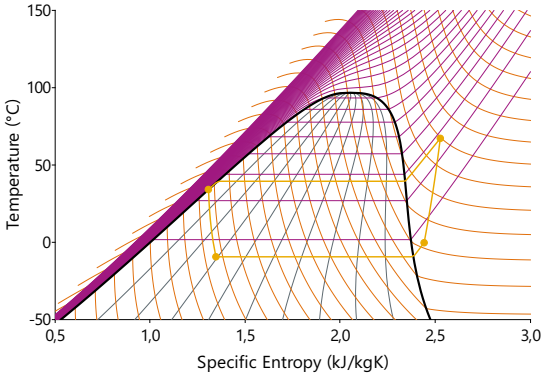


(b) Heat pump cycle in a temperature entropy diagram with isobars in violet, constant enthalpy lines in orange and steam quality in grey.

Figure 5.4: Achieved cycle in Dymola with steady state conditions. Condensing pressure is 13.55 bar and evaporating pressure is 3.49 bar.

[iii] PI controlled
[iv] Input

The superheat of 9.1 K claims roughly 20 % of the evaporator surface to superheating (fig. 5.5a). The temperature difference in the evaporator is approximately 7 °C in the phase changing section and rapidly lowering in the superheating section. In the condenser, the temperature difference is roughly 5 °C through the phase changing section (fig. 5.5b). Approximately 15 % of the heat exchanger area is used for desuperheating and subcooling the refrigerant.

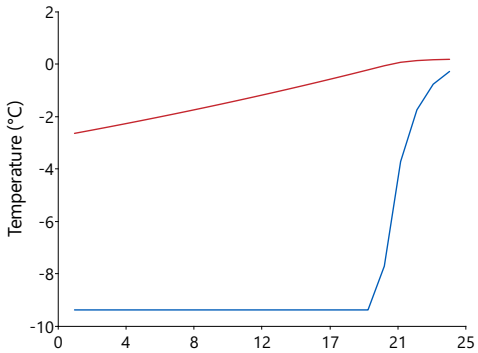


(a) Temperature distribution through the evaporator. The blue line shows R290 fluid temperature, and the red line shows brine temperature. Cell numbers 1 and 24 refer to R290 inlet and outlet, respectively.

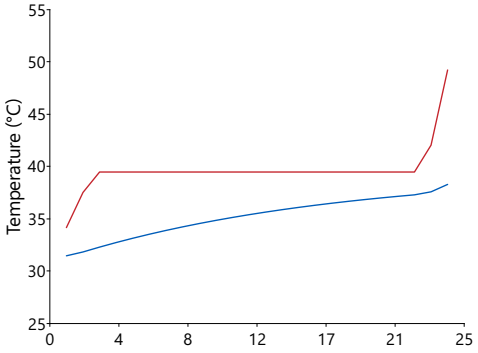


(b) Temperature distribution through the condenser. The blue line shows hydronic liquid temperature, and the red line shows R290 fluid temperature. Cell numbers 1 and 24 refer to hydronic inlet and outlet, respectively.

Figure 5.5: Temperature distribution through heat exchangers in the R290 Dymola model. The vertical axis shows temperature; the horizontal axis shows position by cell number.

## 5.2 R744 Dymola Simulation Campaign

This section will present the results from the simulation campaign conducted and explained in chapter 4. To evaluate the effect of various parameters, the model was simulated with only one changing parameter at a time.

### 5.2.1 Case 1: Ambient Temperature and Heat Source Variation

With the selected pressure losses, the ground heat source simulation shows the best total performance at ambient temperatures below approximately −1 °C (fig. 5.6). Above −1 °C it seems beneficial to include the ambient heat source. The total performance is simulated to be higher in ambient mode than in combined mode for all brine temperatures at ambient heat source exit (fig. 5.6D). In summary, the COP is higher in combination mode for certain temperatures, but the total performance $COP_{tot}$ is highest in ground mode at ambient temperatures below −1 °C and ambient mode at temperatures above −1 °C. The performance fluctuation observed between 0 °C and 5 °C ambient temperature is a result of the peak load heater engaging and disengaging (fig. 5.6A, 5.6C). The fluctuation observed at approximately 0 °C brine temperature is a product of the same process (fig. 5.6B, 5.6D).

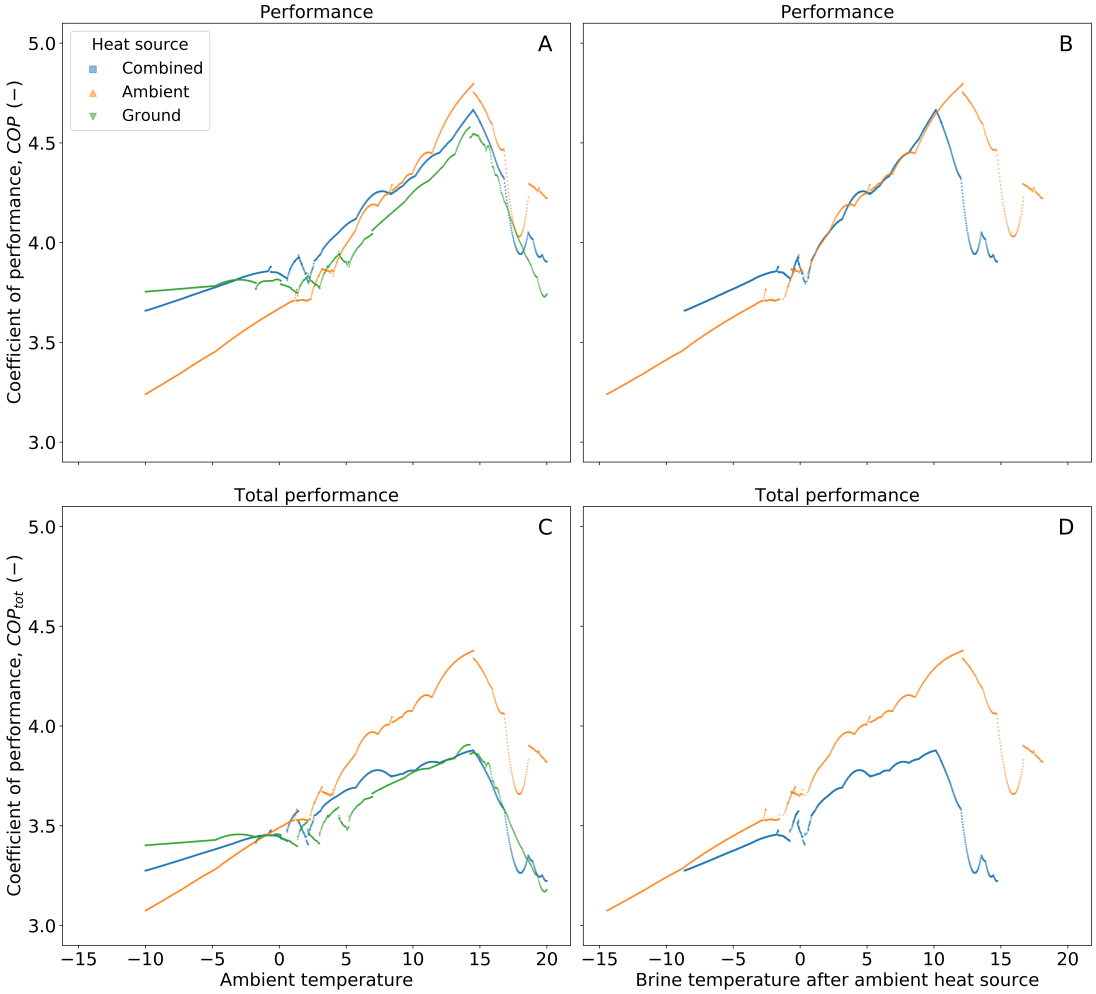


Figure 5.6: Case 1. R744 model performance with different heat sources and varying ambient temperature. Green represents the ground heat source only. Orange represents the ambient heat source only, while blue combines both heat sources.

### 5.2.2 Case 2: Cold Water Temperature Variation

The simulations in case 2 show a less cold water temperature-dependent system when combining DHW and space heating (fig. 5.7). The performance is highly affected by the cold water temperature, but much less so when also producing low temperature space heating. As the cold water mass flow is equal for all compressor frequencies, the $CO_2$ does not reach as low temperatures exiting the last gas cooler.

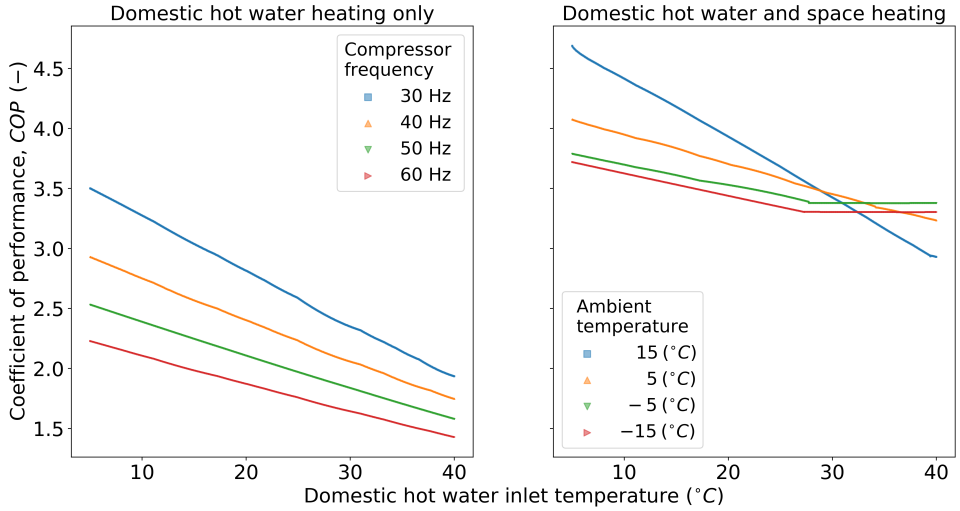


Figure 5.7: Case 2. Cold water inlet temperature effects on the coefficient of performance.

### 5.2.3 Case 3: High Pressure Variation

Case 3 varies the high pressure under diverse boundary conditions. The simulations show the model favours lower high pressures for most simulations, but the DHW heating mode (fig. 5.8). Still, a combination of DHW and space heating gives higher performance. In space heating mode, the COP is considerably lower, ranging from 1.7 to 2.3.

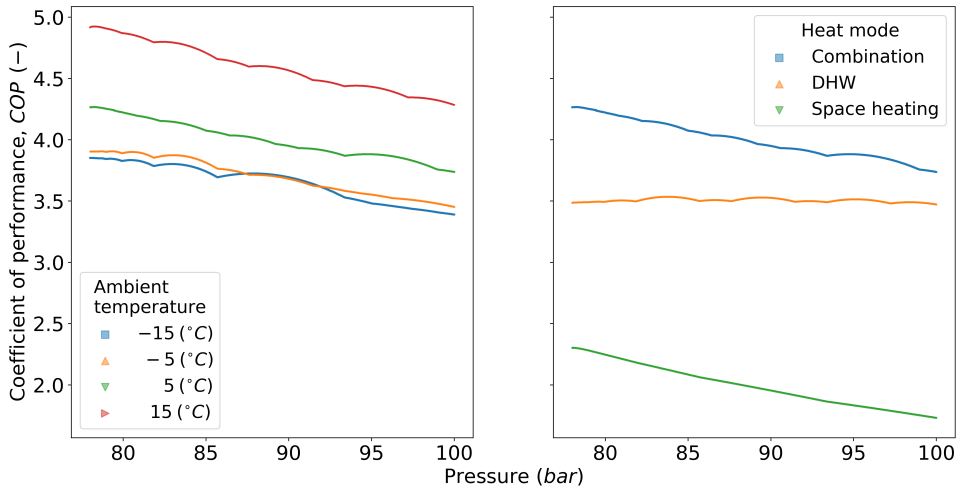


Figure 5.8: Case 3. Effects on performance by high pressure set point when heating domestic water, space heating or both simultaneously and at different ambient temperatures.

### 5.2.4 Case 4: Brine Temperature Variation

The R744 heat pump was not able to deliver sufficient heat to the hydronic water at lower brine temperatures. Therefore the R290 heat pump activated and did not entirely deactivate until the brine temperature entering the R744 heat pump reached −0.2 °C. This is seen as fluctuation in performance, heat production, cooling and hydronic supply temperature (fig. 5.9). The performance increases with an increasing brine temperature in all three heat modes. As the brine temperature reaches about 5 °C, the performance in combination mode flattens at approximately 4.0. The performance in space heating mode shows an inflection point at about 2.5 °C, with a relatively large increase in performance at lower and higher brine temperatures.

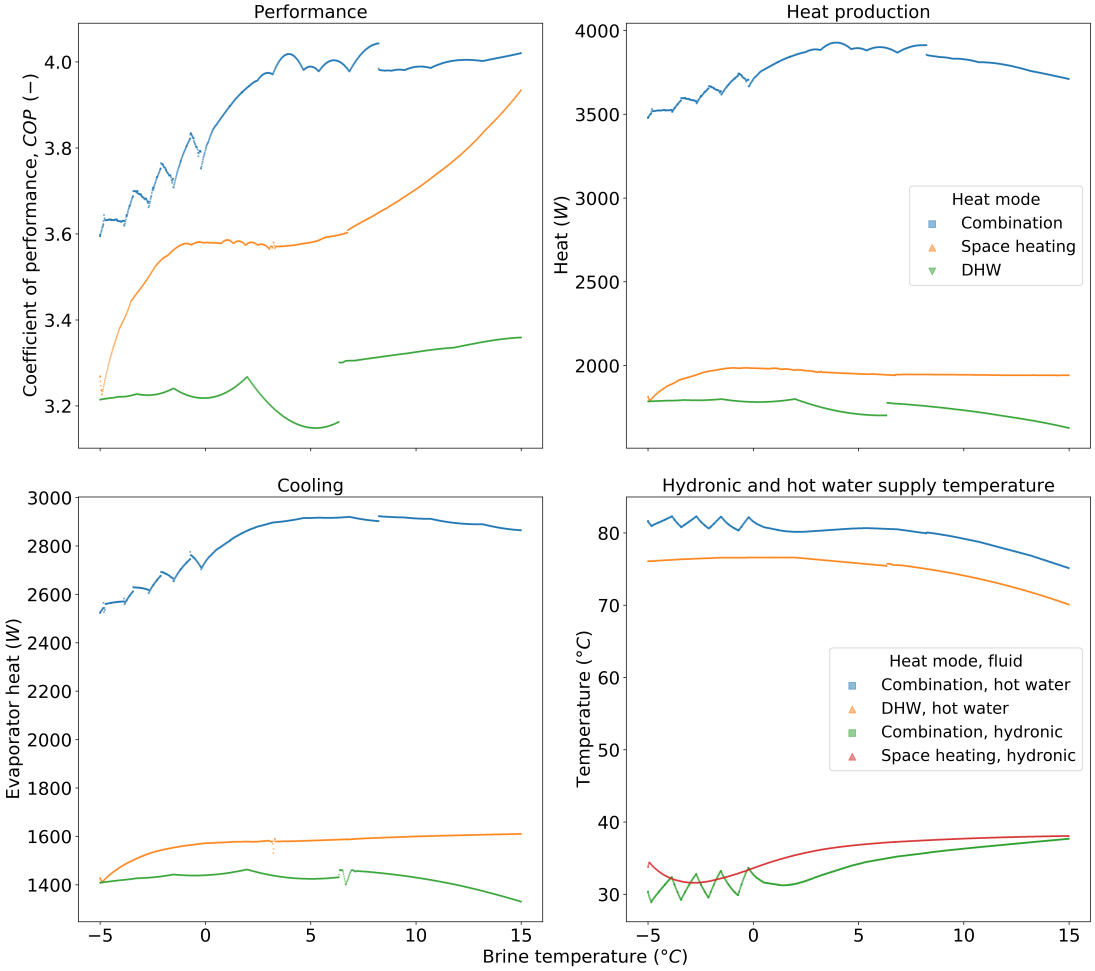


Figure 5.9: Case 4. Effects of changes to brine temperature entering the R744 heat pump on performance, heat production, cooling and product temperatures.

### 5.2.5 Case 5: Hydronic Return Temperature Variation

The simulations show a steep decrease in performance when hydronic return temperature increases past 30 °C (fig. 5.10). The reduction continues in space heating mode, reaching a COP near 1. In combination mode, the performance recovers with a COP reaching 2.5 at a hydronic return temperature of 60 °C. The heat delivered to the hydronic water decreases from approximately 2.3 kW to near nothing in combination mode while in space heating mode producing from about 3.9 kW to 1.5 kW.

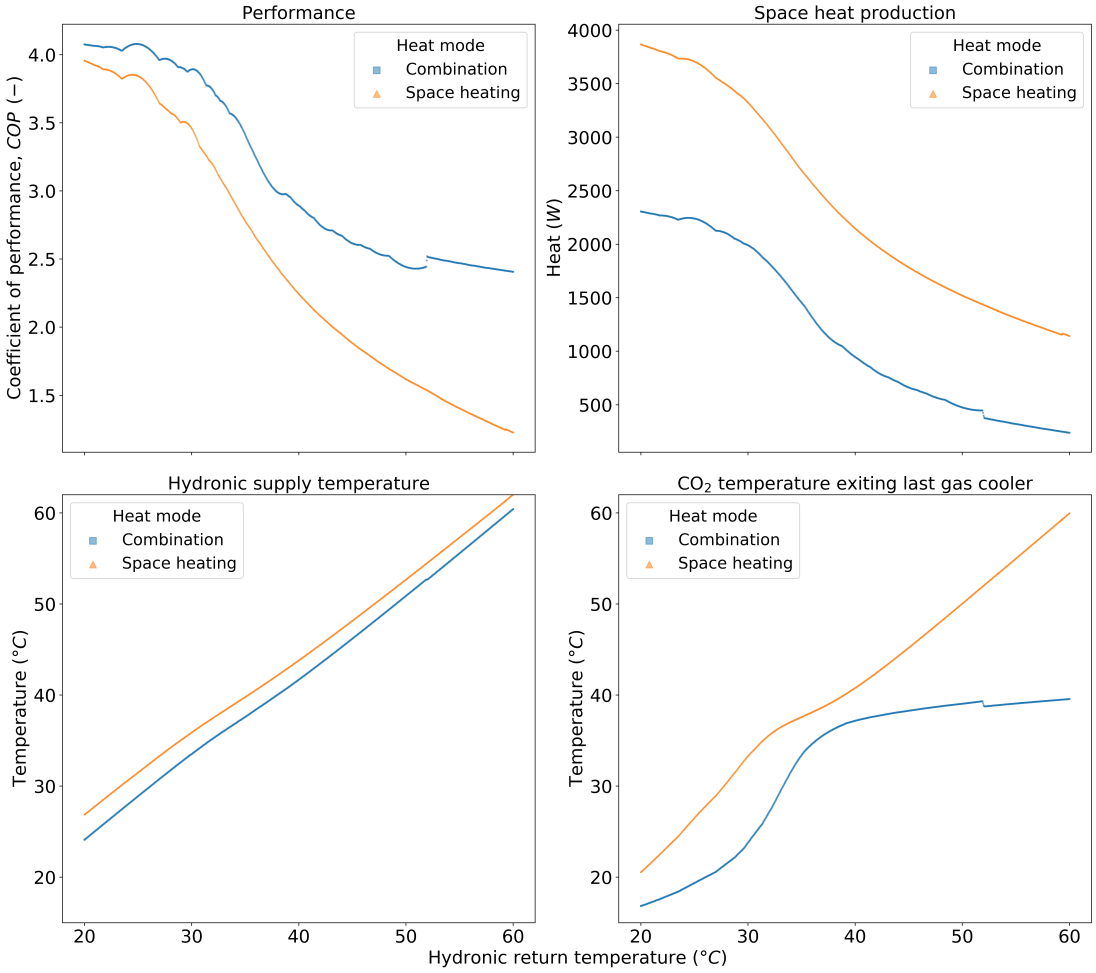


Figure 5.10: Case 5. Effects of changes to hydronic return temperature on performance, space heating, and temperatures.

### 5.2.6 Case 6: Brine Flow Variation

The simulations show only small changes in performance related to the brine mass flow (fig 5.11A). The total performance on the other hand has a peak around $0.13\,\mathrm{kg\,s^{-1}}$ for combination mode and a decreasing total performance with increasing brine flow in the other two heat modes (fig. 5.11B). The brine temperature at R744 evaporator outlet decreases rapidly as the brine flow goes below $0.1\,\mathrm{kg\,s^{-1}}$, reaching temperatures below $-8\,^{\circ}\mathrm{C}$ in combination mode (fig. 5.11C). The low pressure has a similar curve to the brine temperature, with a rapid decrease in pressure as brine flow drop below $0.1\,\mathrm{kg\,s^{-1}}$.

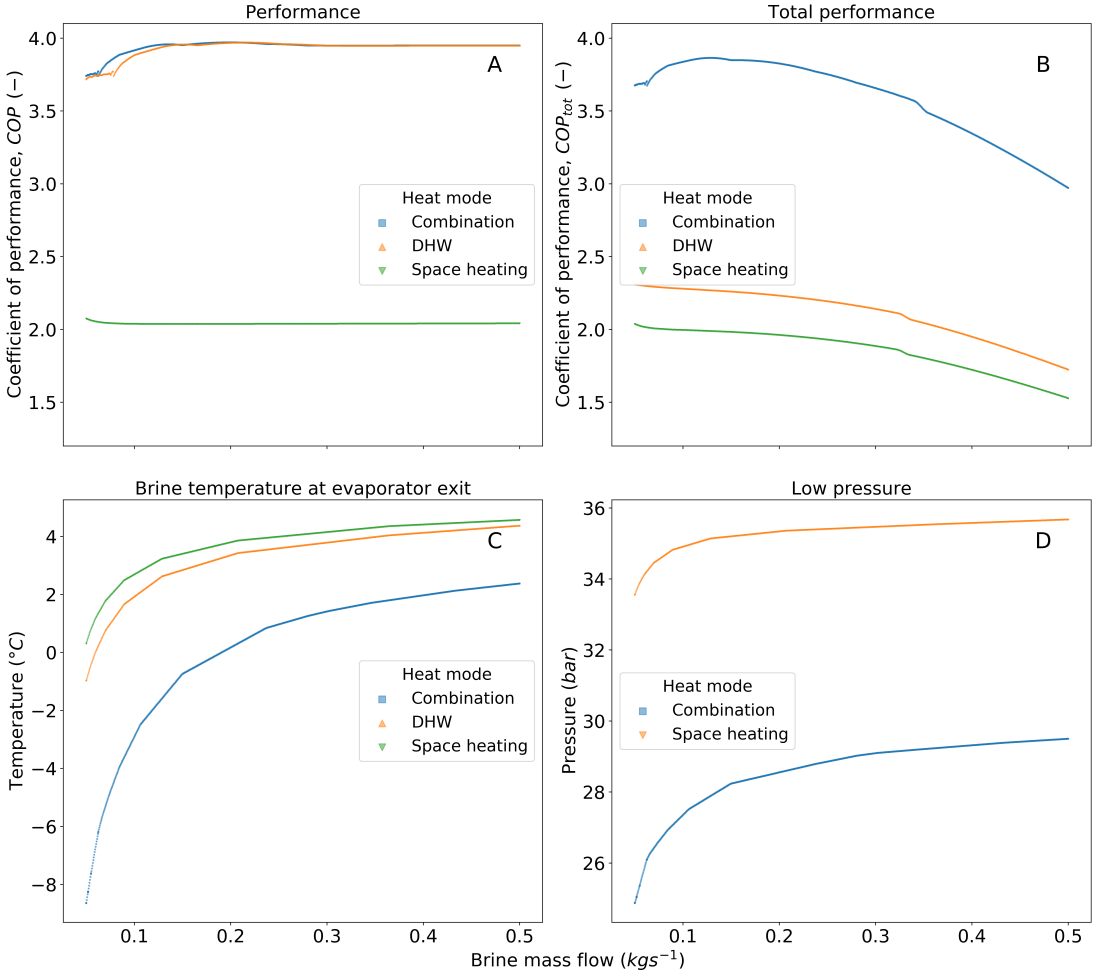


Figure 5.11: Case 6. Effects of changes to brine flow on performance, space heating, and temperatures.

# 6 Discussion

**The Dymola model** developed in this project was validated and showed satisfactory results. It had low deviations from the physical heat pump, and is evaluated to act as a good digital replica. The validation support the use of this model to analyse changes to the heat pump system before actual implementation. The deviations from the physical heat pump are improved through component input modifications, and the system performs adequately in multiple steady state cases. The steady state scenarios ($n = 11$) to which the model has been validated, include both DHW and space heating mode, various compressor frequencies, temperatures and high and low pressures. Uncertainty in temperature measurements and low heat flow in the preheating gas cooler (GC3), made the development of GC3 demanding, but more data from the heat pump gave the basis for creating a well functioning preheating gas cooler.

In order to increase simulation speed, the pressure losses are neglected in the $CO_2$ side of components in this project. Although this has an effect on the process, effort has been put to neglecting the pressure loss where it compromises the simulations the least, while still increasing simulation speed. The low temperature loss from pressure drop ($\delta T/\delta p$) in $CO_2$ gas cooling, keeps the model deviations from physical heat pump limited.

In the brine, hydronic and DHW systems, most pressure drops were constant. This favours higher flow, which in turn skews the total performance presented in Case 1, where heat sources and ambient temperature were varied (fig. 5.6). In Case 6 on the other hand the pressure drops in the brine circuit follows pressure drop models dependant on flow, and are likely to give quite accurate results on effect from brine flow variations. As the heat transfers are only temperature dependent, the total performance ($COP_{tot}$) in Case 6 is skewed, favouring low brine flow (fig. 5.11). Although the simplifications in heat transfer and pressure drop weakens the model validity, the model has proved to behave similar to the heat pump in several steady state scenarios.

**The Dymola simulation campaign** has given data useful for choosing the heat pump controls. In Case 1, three simulations were conducted with an ambient temperature increasing from $-10\,°C$ to $20\,°C$, one for each heat source mode. In these simulations the best total performance ($COP_{tot}$) is found in either ambient mode or ground mode, and never the combination of both heat sources. In fact the performance (COP) was only slightly higher in combination mode at ambient temperatures from approximately $-3\,°C$ to $8\,°C$. The total performance is a result of chosen pressure drops, with lower pressure drops it is more likely that a combination mode is beneficial in a range of ambient temperature. On the other hand, the COP is never much higher in combination mode, which turns for separate use of the heat sources. The combination of heat sources has only been simulated in series. A parallel connection would decrease flow in each source, which in turn reduces pressure drop and pump power. It is possible a parallel connection with flow through both sources could be beneficial for an ambient temperature range within $< -3, 8 >\,°C$.

There is no defrosting in the simulations, and the optimal switching point from ground to

ambient heat source could therefore be higher. An option worth considering when both ambient and ground heat sources are available is to switch to ground heat source when the ambient heat exchanger needs defrosting.

In Case 2, the cold water (CW) inlet temperature was varied from 5 °C to 40 °C in eight simulations. The first four simulations were conducted with domestic hot water (DHW) heating only and controlled compressor frequency input, $f = \{30, 40, 50, 60\}$Hz. As the CW flow was constant, it's ability to cool the $CO_2$ fluid is limited, and as expected the lower frequencies gave a higher performance. The drop in performance with increasing CW temperature is simulated to be near linear and quite steep, ranging from 3.5 to about 1.9 at best. The last four simulations were carried out with given ambient temperatures $T_{amb} = \{-15, -5, 5, 15\}$°C in combination mode, delivering both DHW and space heating. Worth noticing is that the simulation with the highest ambient temperature, holds both the best and the worst performance. With a low CW temperature, the heat pump has a COP above 4.5, but as the CW temperature rises, the COP drops significantly as there is very little heating demand, and the $CO_2$ is not cooled sufficiently. At the lower ambient temperatures on the other hand, the performance stabilises at around 3.4 when the $CO_2$ starts to bypass the preheating gas cooler. The bypass is engaged as the space heating demand cools the $CO_2$ to a lower temperature than the CW.

In Case 3, the high pressure is varied from 78 bar to 100 bar in eight simulations, including given ambient temperatures, $T_{amb} = \{-15, -5, 5, 15\}$°C and all three heat modes; DHW, space heating and combination. All simulations show a decrease in performance with increasing high pressure, except in DHW mode, where the performance is quite constant. One drawback of this approach is the lack of pressure ratio related compressor efficiency. Still the validation process has proven the model compressor to perform with insignificant deviations from the actual heat pump.

In Case 4, the brine temperature was increased from −5 °C to 15 °C in three simulations, covering the three heat modes. In combination mode, the $CO_2$ heat pump (HP) was not able to deliver adequate space heating, and therefore the R290 HP engaged. As the model is designed with very little thermal inertia, the R290 HP is turned on and off multiple times until the brine temperature reaches about 0 °C. This is seen as fluctuations in performance, cooling capacity, heat production and delivered temperatures (fig. 5.9). A peak in heat production and cooling is found in combination mode at a brine temperature of approximately 4 °C, although performance still increases. This could be due to the decrease in hot water supply temperature, as a result of decreased $CO_2$ mass flow and discharge temperature. The performance in space heating mode has an inflection point at around 2.5 °C. A possible explanation for this could be the raised hydronic return temperature from the R290 HP engaging at low brine temperature, from lack of space heating delivered from the $CO_2$ HP. The increase in hydronic return temperature pulls the COP low at low brine temperature. When the R290 HP is turned off again, the hydronic return temperature quickly decreases, which in turn increases the performance rapidly until the system stabilises. In the DHW simulation, the performance makes a jump at approximately 6 °C. At this point, the brine switches change the brine flow to bypass the ground heat source, but as the brine temperature is forced after passing the heat sources,

this has no effect. The performance jump happens as the heat flow in all three gas coolers simultaneously make a small increase ($\Delta Q_{GC1} < 10\,\mathrm{W}$, $\Delta Q_{GC2} \approx \Delta Q_{GC3} \approx 30\,\mathrm{W}$) while the compressor shaft power is steady. The jump in heat flow seems to be a result of a discharge temperature jump of about 0.5 °C. Therefore it seems likely to presume a more linear curve in space heating performance and that the effect between approximately 2 °C and 6 °C is a model and simulation error.

In Case 5, the hydronic return water temperature is increased from 20 °C to 60 °C in two simulations; combination mode and space heating mode. The results show a steep decrease in performance in both simulations when hydronic return temperature rises above approximately 30 °C. This promotes the importance of good space heating system controls.

In case 6, the brine flow is increased from $0.05\,\mathrm{kg\,s^{-1}}$ to $0.50\,\mathrm{kg\,s^{-1}}$ with flow dependant pressure drop models in the brine circuit. Three simulations were conducted, one for each heat mode. The simulations show a low impact from brine flow on performance. The total performance on the other hand, has a peak in combination mode between $0.10\,\mathrm{kg\,s^{-1}}$ and $0.20\,\mathrm{kg\,s^{-1}}$. In the single heat modes the total performance decreases with increasing brine flow within the range simulated. This is likely due to a lower need for heat source capacity in single mode, and a peak should be found at a lower flow. The lack of flow dependant heat transfer coefficients in the model favours a low brine flow, which could be skewing the results. Although the total performance indicate a brine flow in the lower section of the range simulated, the brine temperature at evaporator exit rapidly drops low as flow decreases past $1.5\,\mathrm{kg\,s^{-1}}$.

# 7 Conclusion

There were two main objectives of this thesis. The first, was to develop and implement new heat pump controls in a two-family house heating system and then perform experimental testing using the new control system. The second objective was to develop a digital replica of the heat pump system in Dymola. The heat pump controls were developed through mapping of the current heat pump conditions to evaluate which factors to improve. The process of implementing new controls to the system interface was begun but not completed this semester. Simultaneously, the Dymola model was further modified and validated with various steady state scenarios ($n = 11$).

The process of validating the Dymola model has proven the model can be used to simulate and analyse changes made to the heat pump system before physical implementation. In this project, the ambient heat source and various heat pump controls have been evaluated before implementation. Another component that can be tested and analysed for economic viability is the multi-ejector.

A simulation campaign has been performed with changes to various boundary conditions. The results have given data on how the heat pump system should be controlled when the software developed in this project is implemented. Simulations show simultaneous use of both ground and ambient heat sources is never beneficial. Under relatively high ambient temperatures, simulations indicate it may be beneficial to solely produce space heating when also producing domestic hot water.

Overall the Dymola model proved a useful tool for simulating changes to the system before physical implementation.

# 8 Further work

There are several opportunities for further work. First of all, the implementation of new heat pump controls should be completed. The controls will facilitate experimental studies similar to the simulations performed in this thesis. These experimental studies can include comparing ambient and ground heat sources for optimum switching conditions. Also, one can analyse high pressure optimums for different heat modes. The heat pump controls will most likely improve system performance by utilising the optimums found in simulations and, later, experimental studies.

The propane model could be developed further to better replicate the heat pump in use. Modifications are needed on the evaporator, compressor and condenser. To do this, either information will need to be given by the supplier, or data has to be collected from different steady states, as with the R744 heat pump unit.

The domestic hot water (DHW) system modelled in Dymola should be modified to include accumulator tanks in series with realistic heat transfer within the accumulators. The accumulation system can then be modified to evaluate the effects of mixing and conduction. The current system has four volumes in series, and it would be interesting to see the effects of increasing this without increasing the total volume. Simulations can be performed comparing the current accumulation system and a perfect accumulation system with only cold water entering the heat pump.

A financial calculation on accumulation system improvements should be performed. Then an experimental study on using expansion tanks as DHW accumulators to remove all mixing and conduction should be tested. This means only heated tap water is stored. A system with expansion tanks as DHW accumulators requires a large volume of air, and these tanks are more expensive as there is a higher health risk in containing pressurised air than in pressurised water. Another challenge in this type of accumulation is the varying hot tap water pressure, in contrast to the constant city water pressure.

Financial calculations for the two heat pump applications can be performed. If proven economically beneficial in most residential buildings, a scalable $CO_2$ or propane heat pump could lower the electrical consumption in buildings in colder climates.

# Bibliography

[1] Clare Breidenich, Daniel Magraw, Anne Rowley, and James W Rubin. The Kyoto Protocol to the United Nations Framework Convention on Climate Change. *The American Journal of International Law*, 92(2):315–331, 1998. URL `https://about.jstor.org/terms`.

[2] Produksjon og forbruk av energi, energibalanse og energiregnskap, 6 2021. URL `https://www.ssb.no/energi-og-industri/energi/statistikk/produksjon-og-forbruk-av-energi-energibalanse-og-energiregnskap`.

[3] Asplan Viak and Oslo Economics. Kartlegging og vurdering av potensial for effektivisering av oppvarming og kjøling i Norge. Technical report, NVE, 2020. URL `www.nve.no`.

[4] Gustav Lorentzen. Revival of carbon dioxide as a refrigerant. *International Journal of Refrigeration*, 17(5):292–301, 1 1994. ISSN 01407007. doi: 10.1016/0140-7007(94)90059-0.

[5] Eivind Brodal and Steve Jackson. A comparative study of CO2 heat pump performance for combined space and hot water heating. *International Journal of Refrigeration*, 108:234–245, 12 2019. ISSN 01407007. doi: 10.1016/j.ijrefrig.2019.08.019.

[6] Kashif Nawaz, Bo Shen, Ahmed Elatar, Van Baxter, and Omar Abdelaziz. R290 (propane) and R600a (isobutane) as natural refrigerants for residential heat pump water heaters. *Applied Thermal Engineering*, 127:870–883, 12 2017. ISSN 13594311. doi: 10.1016/j.applthermaleng.2017.08.080.

[7] Paride Gullo, Lorenzo Fusini, and Armin Hafner. *MultiPACK Demonstration of the next generation standardised integrated cooling and heating packages for commercial and public buildings based on environment-friendly carbon dioxide vapour compression cycles IA (Innovation Action) H2020-EE-2016-RIA-IA/ EE-*. 2017.

[8] Yuntao Jiang, Yitai Ma, Minxia Li, and Lin Fu. An experimental study of transcritical CO2 water–water heat pump using compact tube-in-tube heat exchangers. *Energy Conversion and Management*, 76:92–100, 12 2013. ISSN 0196-8904. doi: 10.1016/J.ENCONMAN.2013.07.031.

[9] Ignat Tolstorebrov, Alireza Zendehboudi, Krzysztof Banasiak, Lukas Köster, Ángel Álvarez Pardiñas, and Armin Hafner. Testing of tri-partite CO2 gas cooler prototype for domestic hot water and space heating. *91-96*, 2020-December:153–158, 2020. ISSN 0151-1637. doi: 10.18462/IIR.GL.2020.1120. URL `https://sintef.brage.unit.no/sintef-xmlui/handle/11250/2757361`.

[10] Alireza Zendehboudi, Zuliang Ye, Armin Hafner, Trond Andresen, and Geir Skaugen. Heat transfer and pressure drop of supercritical CO2 in brazed plate heat exchangers of the tri-partite gas cooler. *International Journal of Heat and Mass Transfer*, 178:21, 10 2021. ISSN 00179310. doi: 10.1016/j.ijheatmasstransfer.2021.121641.

[11] Jon Iturralde, Laura Alonso, Angel Carrera, Jaume Salom, Mattia Battaglia, and Daniel Carbonell. Energy demands for multi-family buildings in different climatic zones Deliverable number: D1.1. Technical report, TECNALIA, 9 2019. URL `http://www.tri-hp.eu`.

[12] Jørn Stene. *Residential CO2 heat pump system for combined space heating and hot water heating.* PhD thesis, NTNU, 2004. URL `https://ntnuopen.ntnu.no/ntnu-xmlui/handle/11250/233381`.

[13] Güntner Vertical COMPACT Dry Cooler — Cooling Systems —. URL `https://www.guntner.com/products/dry-coolers/compact/vertical-compact-dc`.

[14] Jorrit, Wronski; Maarten, and Winter. CoolPack - IPU, 2019. URL `https://www.ipu.dk/products/coolpack/`.

[15] Dassault Systems. What is Dymola?, 2019.

# Appendix

# A

## A.1 R744 Heat Pump Pictures

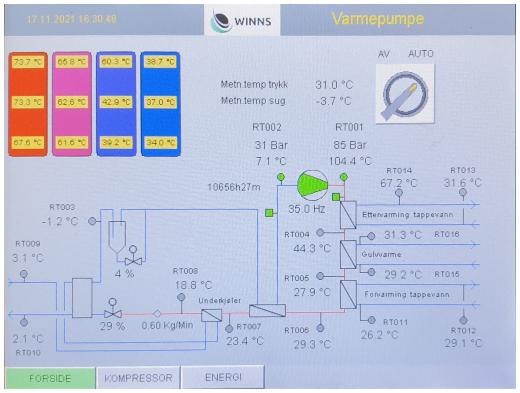


(a)

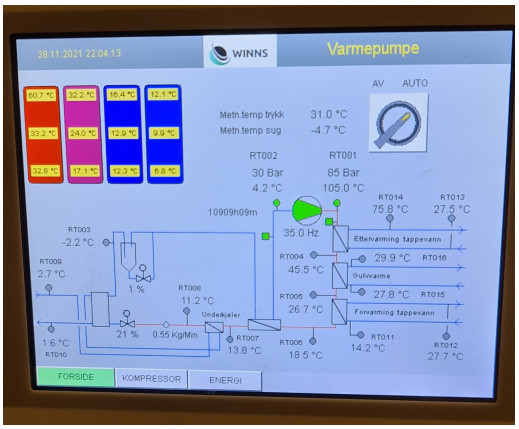


(b)

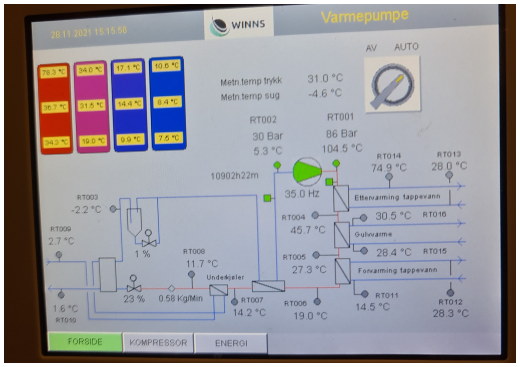


(c)

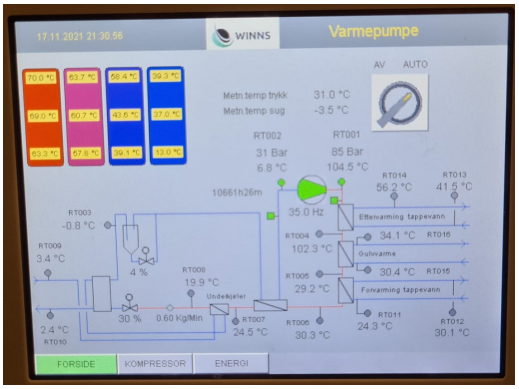


(d)

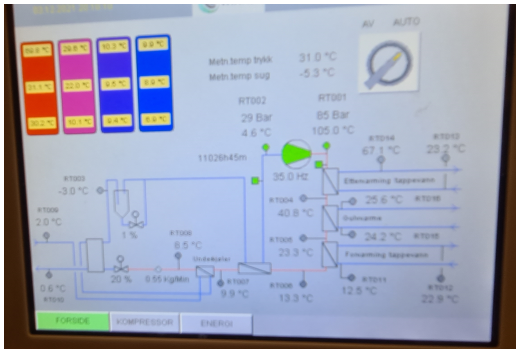


(e)

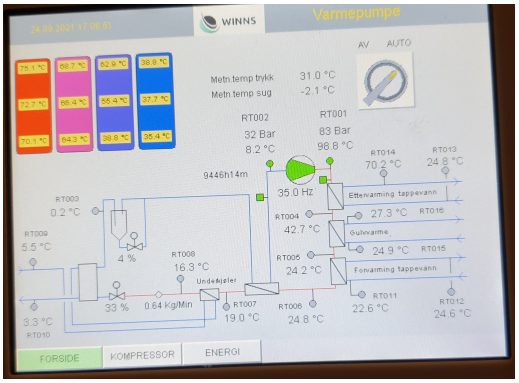


(f)

Figure A.1: Picture of R744 screen during steady state conditions.

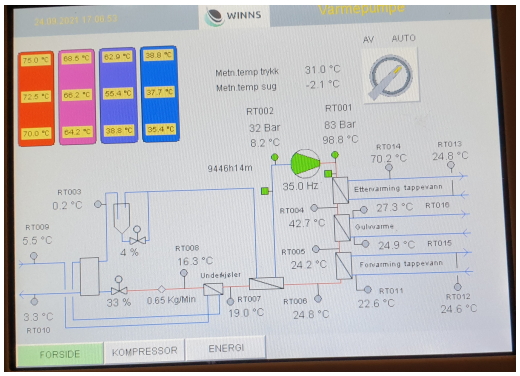


(a)

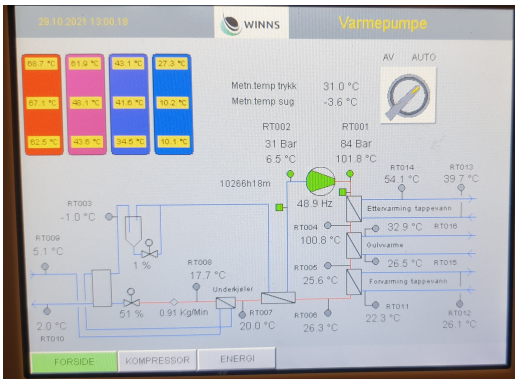


(b)

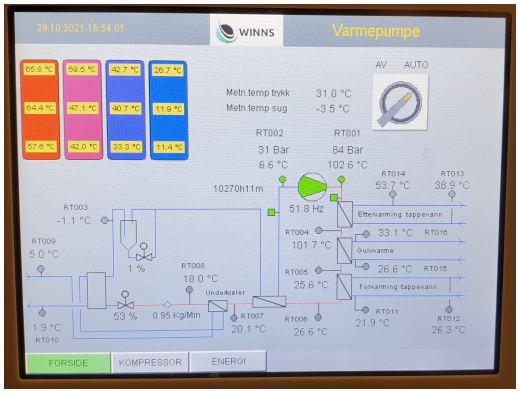


(c)

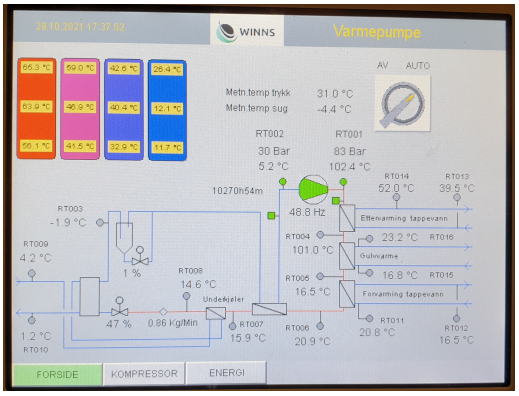


(d)

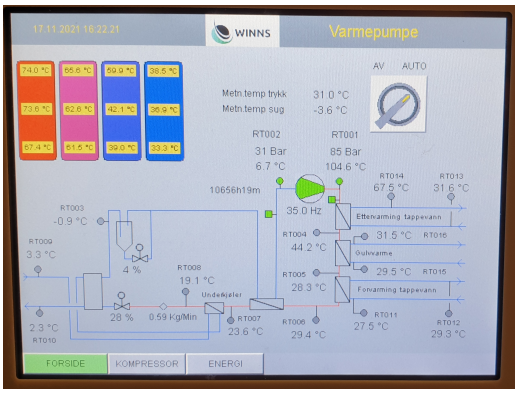


(e)

Figure A.2: Picture of R744 screen during steady state conditions, continued.

## A.2 Ambient Heat Source

Güntner *

NTNU

Date: 2021-12-02
Enquiry dated:
Project: Varmeopptak
Quotation-no.:
Item:
Reference:

| Drycooler | GFVC FD 080.1/11-10 | | |
|---|---|---|---|
| **Capacity:** | 5.0 kW | **Medium:** | Ethanol 35 Vol. %(1) |
| Surface reserve: | 14.2 % | Inlet: | -1.0 °C |
| Air flow: | 3267 m³/h | Outlet: | 5.0 °C |
| Air velocity: | 0.7 m/s | | |
| Air inlet: | 10.0 °C | Pressure drop: | 0.18 bar |
| Altitude: | 0 m | Volume flow: | 0.78 m³/h |
| Air outlet: | 6.9 °C | | |

| | | | |
|---|---|---|---|
| Fans (EC): (VT03062U.1) 1 Piece(s) 1~230V 50-60Hz | | Noise pressure level: | 10 dB(A)(2) |
| Data per motor (nominal data): | | at a distance of: | 10.0 m |
| Speed: | 195 min-1 | Noise power level: | 41 dB(A) |
| Capacity (el.): | 0.03 kW | ErP: | Compliant(3) |
| Current: | 0.15 A(4) | | |
| Total el. power consumption: 0.02 kW | | Energy efficiency class: | A+ (2014) |
| Casing: | Galv. Steel, RAL 7035 | Tubes: | Copper(5) |
| Surface: | 62.2 m² | Fins: | Aluminum(5) |
| Tube volume: | 5.5 l | Connections per unit: | |
| Fin spacing: | 3.00 mm | Inlet: | 16.0 * 1.00 mm |
| Dry weight: | 82 kg(6) | Outlet: | 16.0 * 1.00 mm |
| Max. operating pressure: | 10.0 bar | PED classification: | Art. 4, par. 3(7) |
| | | Passes: | 12 |
| **Dimensions:**(6) | | | |
| Length: | 1284 mm | Outlet header: | 16.0 * 1.00 mm |
| Width: | 608 mm | Inlet header: | 16.0 * 1.00 mm |
| Height: | 1153 mm(6) | Circuits: | 1N |
| No. of legs: | 4 | Distributions: | 5 |

UI: 0096670

Project: Varmeopptak
Quotation-no.:
Item:
GFVC FD 080.1/11-10 Reference:

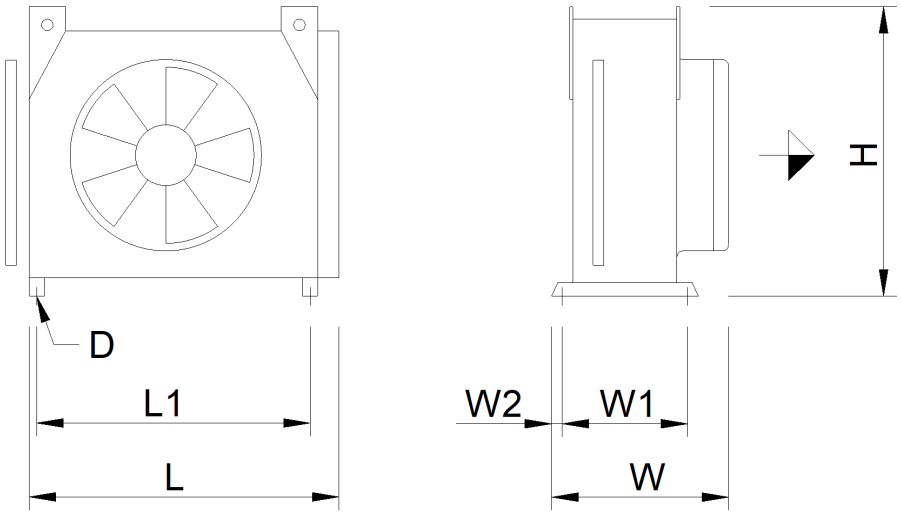


File: EMF\VerticalCompact-BCD_1x1_UNI.emf

| | | | | | | | | |
|---|---|---|---|---|---|---|---|---|
| L | = | 1284 mm | W | = | 608 mm | H | = | 1153 mm |
| L1 | = | 1150 mm | W1 | = | 380 mm | W2 | = | 31 mm |
| D | = | 12.6 mm | | | | | | |

Attention: Drawing and dimensions not valid for all accessory options!

| Accessories | Piece(s) |
|---|---|
| Thread connection R 1/2" Red brass 4243g | 2 |
| Temp. sensor with stainless steel pocket (5209566) | 1 |
| Mounting and wiring (Control cabinet, Fan, Temperature sensor) | 1 |
| GMM(next) EC Controller + GPD[8] | 1 |
| 1 x (5209200) GMM EC-Controller IP54 1xM | |
| 1 x (5209524) Güntner Communication Module GCM (W)LAN GMM EC.1 | |
| 1 x (5215262) GPD+Disconnect RM Box for EC Fans 230VAC 1x | |
| Fan parameterisation omitted[9] | 1 |

**Important remarks / explanatory notes:**

(1) Fluid group 1 according to pressure equipment directive 2014/68/EU

(2) According to the enveloping surface method defined in EN 13487/EN 9614-1; Eurovent tolerance = +2 dB(A). Applies only for AC fans, AC fans with sine control and EC fans. Noise caused by other control methods, water spraying systems or sound reflexions occurring at the installation site are not taken into account and may result in an increased sound pressure level.

(3) This unit is equipped with fans that meet the efficiency requirements of Directive 2009/125/EC (ErP Directive).

(4) The current consumption can differ in dependence of the air temperature and of the variations of system voltage according to the VDE guidance.

(5) The unit may not be suitable for very corrosive atmospheres (close to shores, in smoke rooms, etc.). For further information see program menu "?", "Material recommendations brochure", or ask your sales partner.

(6) Dimensions and weights are not valid for all possible options! They may differ for units with accessories or special units (S-...).

(7) Piping (DN = 14.0 mm, TSmax = 100 °C, liquid). Final classification according to pressure equipment directive 2014/68/EU during order processing.

(8) (GMEC01-0015NO1-xNNxNNN-U-001) Width x Height x Depth: 200 mm x 300 mm x 132 mm, weight: 6 kg, Protect. system IP 54, Operating temperature range: -20.0 °C - 40.0 °C, Power supply: 400 VAC / 5060 Hz / 3-Ph+N+PE, Full load amperage (FLA): 0.1 A, Maximum overload protection (MOP): 10.0 A(gL/gG)

(9) Parametrisation performed automatically by the GMM

**Please pay attention ...**

**There is information for this unit:**

Dangerous refrigerant according to DIN EN 378. Please observe the applicable regulations.

## A.3 Description of Heat Pump System Controls

| Komponent | Komponent-navn | Regulering | Signal inn | Signal ut | Forklaring | Status |
|---|---|---|---|---|---|---|
| Treveis-reguleringsventil | SB001 | Spenning 0/10 | RT011, RT005 | Hovedkort A2, J10 | Hvis RT011>RT005: 0, Hvis ikke: 10 | Eksisterer og programmert |
| Toveis-reguleringsventil | SC002 | Spenning 0-10 | RT014, RT314 | Hovedkort A2, J11 | PID regulering som jobber for å oppnå en varmtvannstemperatur fra varmepumpen . Stengt når sirkulasjonspumpa på tappevann er av. Angitt temperatur bør kunne endres på skjermen. | Ventilen er der, men ikke programmert. |
| Kompressor | JK001 | Frekvens 30-60 | RT016, RT307 (utetemp.) | J14 | Lineær funksjon mellom utetemp. og turtemperatur gulvvarme til huset eller kompressorfrekvens. Setpunkt bør kunne endres på skjermen.<br>T1: Utetemperatur ved frekvens=60<br>T2: Utetemperatur ved frekvens=30<br>Hvis RT307<T1, frekvens=60<br>Hvis RT307>T2, frekvens=30<br>Ellers: Frekvens=30+30*(RT307-T2)/(T1-T2) | Eksisterer og programmert, mangler styring på skjerm. |
| Sirkulasjonspumpe tappevann | JP003 | På/av | RT314 | Hovedkort A2, J18, RELÉ 3 | Av når temperaturen i bunnen av første bereder (der kaldtvann kommer inn) når setpunkt. På når temperatur i bunnen av siste bereder når setpunkt. Setpunkt bør kunne endres på skjermen. | Finnes allerede i elskjema, mangler styring på skjerm. |
| Sirkulasjonspumpe energibrønn | JP004 | Spenning 0-10 | JK001, JK002 | Hovedkort A2, J12 | Pådrag sirk. pumpe justeres etter tre modus: R744 drift, R290 drift eller begge. Setpunkt ved de tre modi bør kunne endres på skjermen. | Finnes allerede i elskjema, mangler styring på skjerm. |
| Sirkulasjonspumpe energibrønn | JP004 | | | Hovedkort A2, J18, RELÉ 4 | Av når begge VP er av, ellers på. | Finnes allerede i elskjema, mangler styring på skjerm. |
| Treveis-reguleringsventil | SB003 | Spenning 0/10 | RT307 | | Henter varme fra uteluft når utetemperatur når setpunktet. Setpunkt bør kunnes justeres. | Helt nytt, ikke montert eller programmert. |
| Høytrykk R744 | | | JP003 eller RT314 | | To setpunkt: a) ved VV produksjon, b) ved kun gulvvarme produksjon. Setpunktene bør kunne endres på skjermen. | Finnes stepventil på A2 J8. Mangler styring på skjerm. |
| Delay | | | RT014 | | Stans (feilmelding) ved høy vanntemperatur ut av reheater bør ha en forsinkelse for å unngå stans av varmepumpen rett etter oppstart av tappevannsproduksjon når anlegget tidligere kun produserte gulvvarme. | Stans ved høy vanntemperatur finnes. Mangler forsinkelse. |
| Energimåler strøm til pumpe energibrønn | | | | BUS | Vises på skjerm. | Helt nytt, ikke montert eller programmert. |
| Energimåler strøm levert til R290 VP | | | | BUS | Vises på skjerm. | Helt nytt, ikke montert eller programmert. |
| Energimåler varme levert fra R290 VP | | | | BUS | Vises på skjerm. Node adresse: 20 | Helt nytt, ikke montert eller programmert. |
| Energimåler gjenvinner avkast | | | | BUS | Vises på skjerm. | Helt nytt, ikke montert eller programmert. |
| Målestasjon R290 | | | RT401-RT408 | | Temperaturfølere på R290 VP. Bør vises på skjerm.<br>RT0: R290 Brine inngang<br>RT1: R290 Brine utgang<br>RT2: R290 Fordamper inngang<br>RT3: R290 Fordamper utgang<br>RT4: R290 Kondensator inngang<br>RT5: R290 Kondensator utgang<br>RT6: R290 Gulvvarme inngang<br>RT7: R290 Gulvvarme utgang | Helt nytt, ikke montert eller programmert. |

| | | | | | | |
|---|---|---|---|---|---|---|
| Målestasjon varmeopptak | | | RT501-508 | | Temperaturfølere på kald side<br>RT0: Varmeveksler ute inngang<br>RT1: Varmeveksler inne inngang<br>RT2: Varmeveksler mot avkast ventilasjon inngang<br>RT3: Varmeveksler mot avkast ventilasjon utgang<br>RT4:<br>RT5:<br>RT6:<br>RT7: | Helt nytt, ikke montert eller programmert. |
| R290 VP | | | | Hovedkort A2, J18, RELÉ 2 | R744 VP kaller R290 for spisslast gulvvarme når RT016<setpunkt. Her kan det også gjerne være en forsinkelse i start av R290 VP. Setpunkt bør kunne endres på skjermen. Forsinkelse som kan endres under "konfigurasjon" siden. Eget setpunkt for av også, da og med forsinkelse. Forsinkelsene kan løses sånn:<br>TimerHighTemp: teller når RT016 (turtemp gulvvarme fra R744) > setpunkt.<br>TimerLowTemp: teller når RT016 < setpunkt.<br>When TimerHighTemp > 600 then Start<br>elsewhen TimerLowTemp > 1800 then Stop | Finnes. Mangler styring fra skjerm og noe programmering. |
| Treveis-reguleringsventil | SB002 | Spenning 0/10 | | Hovedkort A2, J18, RELÉ 2 | Åpner for brine flow gjennom R290 når R744 kaller på spisslast. | Helt nytt. Men relé 2 J18 kaller på spisslast i elskjema, så foreslår å hente fra der. Hvis de ikke skal komme fra samme, kan det være greit å ha en delay på ventilen så det er flow helt til R290 har stoppet. |
| Sirkulasjonspumpe gulvvarme | JP001 | | Inndata, skjerm | Hovedkort A2, J12 | Setpunkt bestemt på skjerm. | Finnes. Mangler styring på skjerm. |
| Kompressor | JK001 | Frekvens 30-60 | Inndata, skjerm | J14 | Overstyring av frekvens, input på skjerm. Beholder også sugeside styring, sånn som den er i dag, men bryter for å velge mellom de tre alternativene:<br>1. Konstant frekvens<br>2. Lineær funksjon av utetemperatur<br>3. Sugesidestyring som i dag. | Finnes. Mangler styring på skjerm/programmering. Usikker på om det er J14 som er utgangen. |

## A.4 Heat Pump Monitor Display Proposition

Sendt 28.02.2022

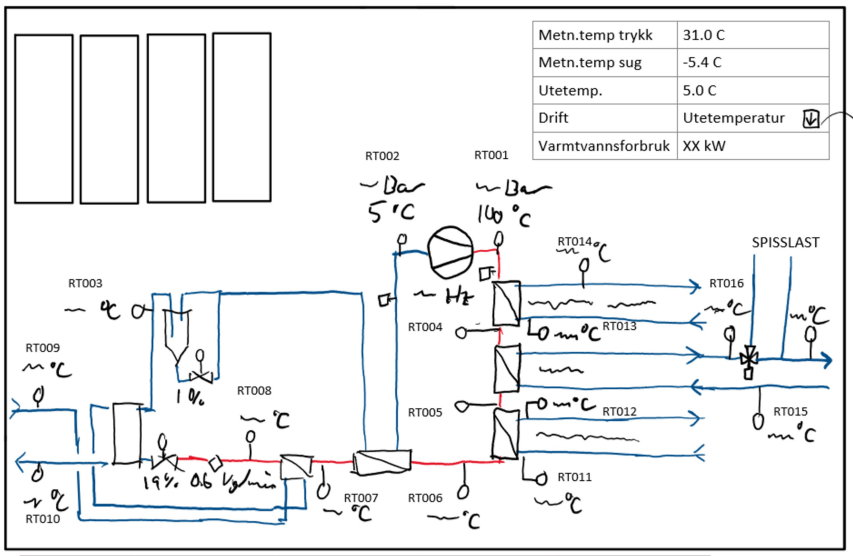


| **FORSIDE** | KONFIGURASJON | ENERGI | SPISSLAST | VARMEKILDE |
|---|---|---|---|---|

| | |
|---|---|
| SETTPUNKT UTEKOMPENSERING | |
| TEMPERATUR VED 30 Hz | 0 |
| TEMPERATUR VED 60 Hz | 15 |
| SETTPUNKT TEMPERATUR SUGESIDE | -4 |
| SETTPUNKT KONSTANT FREKVENS | 32 |
| SETTPUNKT VARMTVANN UT AV GASSKJØLER | 75 |
| SIRK. PUMPE VARMTVANN AV NÅR RT104 > | 40 |
| SIRK. PUMPE VARMTVANN PÅ NÅR RT103 < | 95 |
| BRØNNPUMPE, PÅDRAG VED R744 DRIFT | 35% |
| BRØNNPUMPE, PÅDRAG VED R290 DRIFT | 50% |
| BRØNNPUMPE, PÅDRAG VED R744 & R290 DRIFT | 90% |
| HØYTRKK VED VV PRODUKSJON | 85 |
| HØYTRYKK VED KUN GULVVARME PRODUKSJON | 77 |
| SPISSLAST PÅ NÅR RT016 < | 30 |
| SPISSLAST AV NÅR RT016 > | 35 |
| DELAY SPISSLAST (MINUTTER) | 60 |
| SIRK. PUMP GULVVARME, PÅDRAG | 80% |
| VARMEKILDE UTE NÅR UTETEMPERATUR > | 5 |
| SIRK. PUMPE GULVVARME PÅDRAG | 50% |

| FORSIDE | **KONFIGURASJON** | ENERGI | SPISSLAST | VARMEKILDE |
|---|---|---|---|---|

R744

| | EFFEKT | ENERGI | Annet |
|---|---|---|---|
| KOMPRESSOR | 0.6 kW | 600 kWh | |
| FORDAMPER | 1.0 kW | 1100 kWh | |
| GULVVARME | 0.5 kW | 1200 kWh | 482 l/h |
| VARMTVANN | 1.1 kW | 500 kWh | 23 l/h |
| COP | 2.7 | 2.8 | |

R290

| | EFFEKT | ENERGI | Annet |
|---|---|---|---|
| KOMPRESSOR | 1.0 kW | 400 kWh | |
| FORDAMPER | 2.0 kW | 800 kWh | |
| GULVVARME | 3.0 kW | 1200 kWh | 482 l/h |
| VARMTVANN | | | |
| COP | 3.0 | 3.0 | |

| | EFFEKT | ENERGI | ANNET |
|---|---|---|---|
| UTEVIFTE | 0.5 kW | 230 kWh | 800 l/h |
| ENERGIBRØNN | 0.9 kW | 490 kWh | 800 l/h |

| FORSIDE | KONFIGURASJON | **ENERGI** | SPISSLAST | VARMEKILDE |
|---|---|---|---|---|

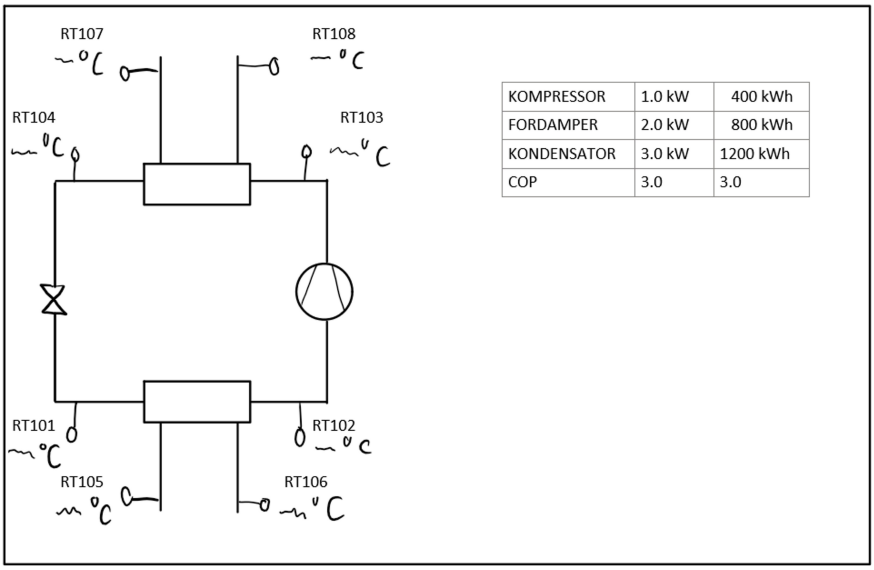


| | | |
|---|---|---|
| KOMPRESSOR | 1.0 kW | 400 kWh |
| FORDAMPER | 2.0 kW | 800 kWh |
| KONDENSATOR | 3.0 kW | 1200 kWh |
| COP | 3.0 | 3.0 |

| FORSIDE | KONFIGURASJON | ENERGI | **SPISSLAST** | VARMEKILDE |
|---|---|---|---|---|

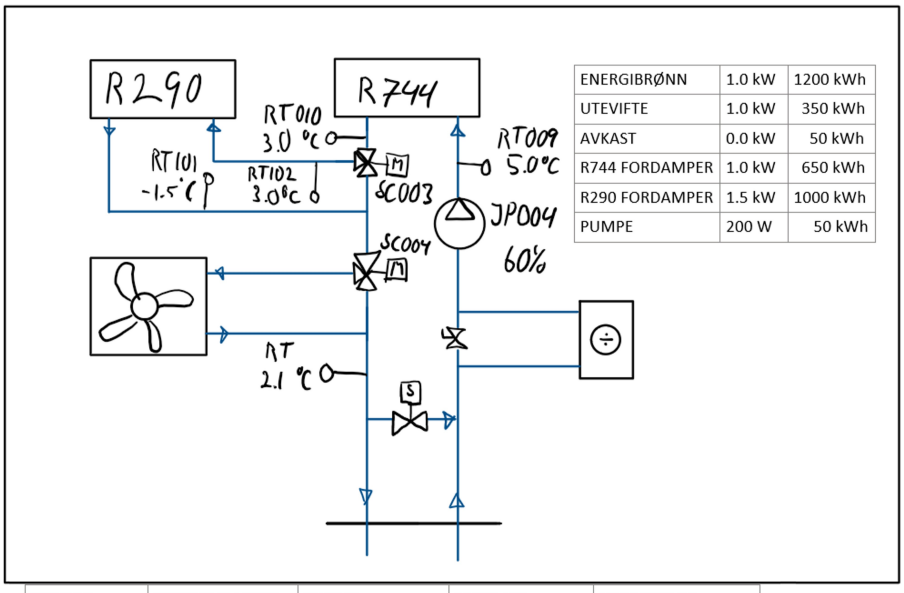


| | | |
|---|---|---|
| ENERGIBRØNN | 1.0 kW | 1200 kWh |
| UTEVIFTE | 1.0 kW | 350 kWh |
| AVKAST | 0.0 kW | 50 kWh |
| R744 FORDAMPER | 1.0 kW | 650 kWh |
| R290 FORDAMPER | 1.5 kW | 1000 kWh |
| PUMPE | 200 W | 50 kWh |

| | | | | |
|---|---|---|---|---|
| FORSIDE | KONFIGURASJON | ENERGI | SPISSLAST | **VARMEKILDE** |

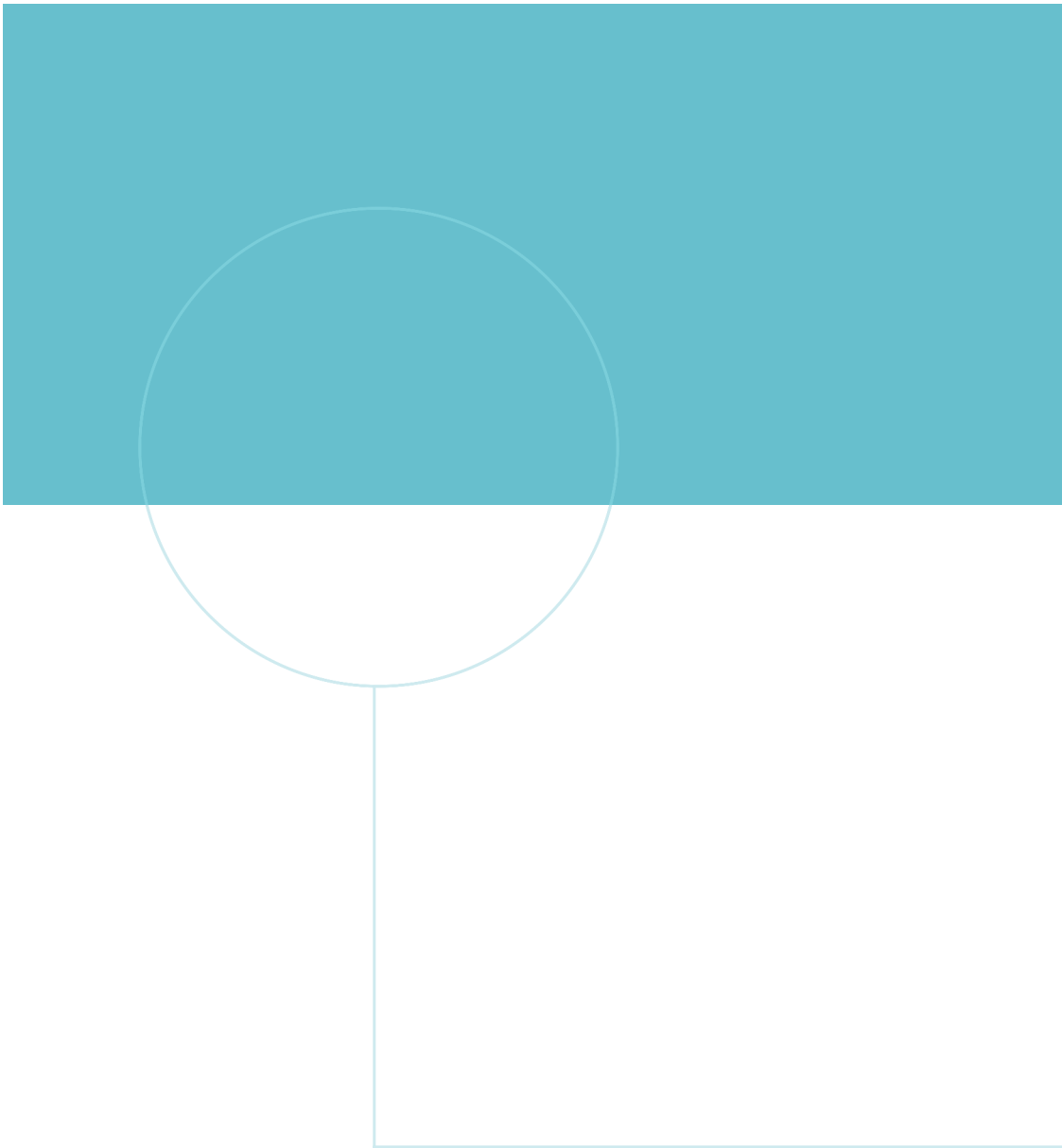

NTNU

Norwegian University of
Science and Technology